Continuous anisotropic damage as a twin modelling of discrete bi-dimensional fracture

C Oliver-Leblond, R Desmorat, Boris Kolev

Continuous anisotropic damage as a twin modelling of discrete bi-dimensional fracture

C. Oliver-Leblond, R. Desmorat, B. Kolev

Université Paris-Saclay, ENS Paris-Saclay, CNRS, LMT - Laboratoire de Mécanique et Technologie, 91190, Gif-sur-Yvette, France

Abstract

In this contribution, the use of discrete simulations to formulate an anisotropic damage model is investigated. It is proposed to use a beam-particle model to perform numerical characterization tests. Indeed, this discrete model explicitly describes cracking by allowing displacement discontinuities and thus capture crack induced anisotropy.

Through 2D discrete simulations, the evolution of the effective elasticity tensor for various loading tests, up to failure, is obtained. The analysis of these tensors through bi-dimensional harmonic decomposition is then performed to estimate the tensorial damage evolution. As a by-product of present work we obtain an upper bound of the distance to the orthotropic symmetry class of bi-dimensional elasticity.

Keywords: Anisotropic Damage, Crack Density, Harmonic Decomposition, DEM, Beam-Particle, Lattice, Discrete simulation

Introduction

For most quasi-brittle materials, the initial mechanical behaviour of the uncracked material can be considered as isotropic. On the other hand, degradation induced by mechanical loading generally leads to anisotropy. Indeed, cracks are naturally oriented and therefore their appearance will not affect the material properties in an isotropic manner. We note that the orientation of these cracks for an initially isotropic material can be determined by the direction and sign of the loading (Mazars et al., 1990; Ramtani et al., 1992).

To obtain an explicit representation of cracking – and thus of its impact on material properties – it is possible to use discrete models of the lattice or particle type. The first lattice models were historically introduced by Poisson (1828) and more recently by Hrennikoff (1941) to solve classical elasticity problems. The elastic material is discretized using 1D elements – springs or beams – which allow for the transfer of forces between the nodes of the lattice. The development of numerical simulations has allowed for its extension to the study of fracture behaviour by considering a brittle behaviour for the elements forming this lattice (Herrmann et al., 1989). The approach was then applied to the quasi-brittle fracture of concrete subjected to tension (Schlangen and Van Mier, 1992). However, these models do not allow for the representation of compression cracking nor of cyclic loading. Particulate models were proposed in 1979 to study the behaviour of granular (Cundall and Strack, 1979) joints. For these applications, contact forces alone were sufficient to correctly describe the behaviour. A cohesive version has been proposed latter (Meguro and Hakuno, 1989) but does not offer the simplicity and rapidity of the lattice models. In the present work, we propose to use a beam-particle model combining the lattice approach and the particulate approach (D'Addetta et al., 2002; Delaplace, 2008; Vassaux et al., 2016). Concrete is represented via an assembly of polygonal particles bounded together by brittle beams. After the beams break, frictional contact forces are introduced between the particles. This model allows for a fine and explicit description of the cracking and the associated mechanisms (initiation, propagation, closure with stiffness recovery, friction). Its application to structural calculations is not yet common but can be envisaged with the implementation of high-performance calculation techniques. These discrete methods can be used as numerical experimentation tools at the scale of the Representative Elemental Volume or at the scale of a laboratory specimen to establish and identify the constituent equations of a continuous model (Vassaux et al., 2015a) or simply a part of these equations (Delaplace and Desmorat, 2007).

In order to obtain a representative, robust and efficient numerical model, it is common to use macroscopic laws that account for the formation, propagation and coalescence of micro-cracks by introducing an internal damage variable. One of the first damage models for quasi-brittle materials (Mazars, 1984) made it possible to reproduce the degradation of the concrete material with loading, via a scalar damage variable, by considering concrete as a homogeneous material at the scale of the volume element

Email addresses: cecile.oliver@ens-paris-saclay.fr (C. Oliver-Leblond), rodrigue.desmorat@ens-paris-saclay.fr (R. Desmorat), boris.kolev@math.cnrs.fr (B. Kolev)

of continuum mechanics. This isotropic damage model is commonly used to study the behaviour of concrete structures but its isotropic nature does not allow for it to take into account complex multi-axial loading (as observed by Mazars and his collaborators, Ramtani et al. (1992), see also the work of Halm and Dragon (1998)). To tackle this issue, damage models with induced anisotropy – such as the one proposed by Desmorat et al. (2007) and made more robust later (Desmorat, 2016) – can be used. In this model, developed within the framework of the thermodynamics of irreversible processes, the damage is represented by a tensor variable of order 2. It should be noted that these macroscopic models are globally phenomenological because their formulation and identification are based on experimental observations of the behaviour of quasi-brittle materials. It is the same for their laws of evolution (Ramtani et al., 1992; Lemaitre and Desmorat, 2005) or their non-local character. Their representativeness is thus limited by the capacity to carry out experiments on the degraded material.

Discrete cracking models and continuous damage models both have advantages and limitations, and it makes sense to combine these advantages by combining the two modelling methods. In this paper, we investigate the relevance to use the beam-particle model to perform virtual tests in order to formulate an anisotropic damage model. Let us recall that in (Delaplace and Desmorat, 2007) the methodology was limited to the identification of a single parameter of the continuous model (certainly delicate to measure on real tests because it was the one governing the so-called "shear-bulk" coupling of a more important effect of the damage on compressibility than on shear). More recent studies have proposed the formulation of continuous damage models from a discrete analysis: by introducing scalar damage variables calculated from the macroscopic loss of stiffness in a lattice simulation (Rinaldi and Lai, 2007; Rinaldi, 2013; Jivkov, 2014), or by continualization of discrete equations (Challamel et al., 2015).

In this paper, the goal is to derive a tensorial damage variable from discrete simulations. The tools for the intrinsic analysis of tensors, introduced by Backus (1970) in elasticity and by Leckie and Onat (1981) in damage mechanics, mixing harmonic analysis and the notion of covariants (generalizing that of invariants, Olive et al. (2018b)), are used here in order to analyze the effective elasticity tensors obtained through discrete simulations, without reference to a particular basis, and to achieve a general tensorial representation of damage. Discrete simulations will be used to obtain the evolution of the effective elasticity tensor during the rupture of a numerical specimen under different mechanical loads. The analysis of the tensors via the harmonic decomposition and their covariant reconstruction (Olive et al., 2018a) will then allow us to estimate the evolution of the tensor damage.

In section 1, definitions relating to the properties of fully symmetrical tensors are recalled. The harmonic decomposition of a bi-dimensional elasticity tensor is then performed in section 2 and it is reminded that the fourth order harmonic part of this elasticity tensor is always an *harmonic square*. In section 3, a covariant reconstruction of 2D orthotropic elasticity tensors is used to derive an upper bound of the distance to the orthotropic symmetry class in bi-dimensional elasticity. The beam-particle model, used in this contribution as a numerical testing tool, is presented in section 4 as well as the methodology to extract the effective elasticity tensor from the discrete simulations. A first analysis is realised in section 5 to check whether the initial elasticity tensor, of the uncracked medium, can be considered as isotropic. In section 6, the analysis of the effective elasticity tensors – and more precisely of their harmonic part – of cracked media for various loading test up to failure is achieved. Finally, the analysis of those tensors through harmonic decomposition/covariant reconstruction is then performed in section 7 to estimate the tensorial damage evolution.

1. Definitions

We next make use of the Euclidean structure of $\mathbb{R}^d$, $d = 2, 3$, and do not make difference between covariant, contravariant or mixed tensors.

1.1. Symmetric tensor product

We denote by $\mathbf{T}^{\mathrm{s}}$ the totally symmetric part of a possibly non symmetric tensor $\mathbf{T}$. More precisely, if $\mathbf{T} \in \otimes^n \mathbb{R}^d$ is of order n,

$$\mathbf{T}^{\mathrm{s}}(\boldsymbol{x}_1, \dots, \boldsymbol{x}_n) := \frac{1}{n!} \sum_{\sigma \in \mathfrak{S}_n} \mathbf{T}(\boldsymbol{x}_{\sigma(1)}, \dots, \boldsymbol{x}_{\sigma(n)}),$$

where $\mathfrak{S}_n$ is the permutation group of n elements.

The *symmetric tensor product* of two tensors $\mathbf{T}_1$ and $\mathbf{T}_2$, of respective orders n_1 and n_2, is the symmetrization of $\mathbf{T}_1 \otimes \mathbf{T}_2$, defining a totally symmetric tensor of order $n = n_1 + n_2$:

$$\mathbf{T}_1 \odot \mathbf{T}_2 := (\mathbf{T}_1 \otimes \mathbf{T}_2)^{\mathrm{s}}.$$

1.2. Traces – Harmonic tensors

Contracting two subscripts i, j of a tensor $\mathbf{T}$ of order n defines a new tensor of order $n-2$ denoted as $\mathrm{tr}_{ij}\,\mathbf{T}$. For a totally symmetric tensor $\mathbf{T}$, this operation does not depend on a particular choice of the pair i, j. Thus, we can refer to this contraction just as the *trace* of $\mathbf{T}$ and we will denote it as $\mathrm{tr}\,\mathbf{T}$. It is a totally symmetric tensor of order $n-2$. Iterating the process, we define

$$\mathrm{tr}^k\,\mathbf{T} = \mathrm{tr}(\mathrm{tr}(\cdots(\mathrm{tr}\,\mathbf{T}))),$$

which is a totally symmetric tensor of order $n - 2k$.

Harmonic tensors $\mathbf{H}$ are by definition totally symmetric traceless tensors, *i.e.* such as $\mathbf{H} = \mathbf{H}^s$, $\mathrm{tr}^k\,\mathbf{H} = 0$. Their vector spaces are denoted $\mathbb{H}^n(\mathbb{R}^d)$, with n the order of considered tensor, d the dimension. In 2D ($d = 2$), $\dim \mathbb{H}^n(\mathbb{R}^2) = 2$, while in 3D ($d = 3$), $\dim \mathbb{H}^n(\mathbb{R}^3) = 2n + 1$. The harmonic tensors of order two (*i.e.* the deviatoric tensors) will be denoted by lowercase letter $\mathbf{h}$.

1.3. Harmonic product

Let $\mathbf{H}_1$ and $\mathbf{H}_2$ be two harmonic tensors of orders n_1 and n_2 respectively. The harmonic product $\mathbf{H}_1 * \mathbf{H}_2$, defining an harmonic tensor of order $n = n_1 + n_2$, has been introduced in (Olive et al., 2018a) as the leading harmonic part of the symmetric tensor product $\mathbf{H}_1 \odot \mathbf{H}_2$,

$$\mathbf{H}_1 * \mathbf{H}_2 := (\mathbf{H}_1 \odot \mathbf{H}_2)' \in \mathbb{H}^{n_1+n_2}(\mathbb{R}^d), \qquad d = 2, 3.$$

In previous works, the leading harmonic part was sometimes denoted $(\mathbf{H}_1 \odot \mathbf{H}_2)_0$. As it is a generalization of the deviatoric part, the notation $(\cdot)'$ is here preferred to $(\cdot)_0$. It is computed at any order thanks to the harmonic decomposition (see section 2). The harmonic product is *associative* and *commutative*,

$$\mathbf{H}_1 * (\mathbf{H}_2 * \mathbf{H}_3) = (\mathbf{H}_1 * \mathbf{H}_2) * \mathbf{H}_3, \quad \mathbf{H}_1 * \mathbf{H}_2 = \mathbf{H}_2 * \mathbf{H}_1.$$

Let us particularize the harmonic product for specific cases of bi-dimensional (2D) vectors and harmonic second-order tensors (belonging thus to $\mathbb{H}^n(\mathbb{R}^2)$ for $n = 1, 2$).

Example 1.1. For two vectors $\boldsymbol{w}_1, \boldsymbol{w}_2 \in \mathbb{H}^1(\mathbb{R}^2)$, we have

$$\begin{aligned}\boldsymbol{w}_1 * \boldsymbol{w}_2 =& (\boldsymbol{w}_1 \odot \boldsymbol{w}_2)' \\ =& \frac{1}{2}(\boldsymbol{w}_1 \otimes \boldsymbol{w}_2 + \boldsymbol{w}_2 \otimes \boldsymbol{w}_1) - \frac{1}{2}(\boldsymbol{w}_1 \cdot \boldsymbol{w}_2)\,\mathbf{1},\end{aligned}$$

where $\boldsymbol{w}_1 \cdot \boldsymbol{w}_2 = \boldsymbol{w}_1^T \boldsymbol{w}_2$ is the scalar product.

Example 1.2. For two second-order harmonic (deviatoric) tensors $\mathbf{h}_1, \mathbf{h}_2 \in \mathbb{H}^2(\mathbb{R}^2)$, we have (Olive et al., 2018a)

$$\begin{aligned}\mathbf{h}_1 * \mathbf{h}_2 =& (\mathbf{h}_1 \odot \mathbf{h}_2)' \\ =& \mathbf{h}_1 \odot \mathbf{h}_2 - \frac{1}{4}\operatorname{tr}(\mathbf{h}_1\mathbf{h}_2)\mathbf{1} \odot \mathbf{1}.\end{aligned}$$

Example 1.3. The harmonic square of a 2D second order harmonic (deviatoric) tensor $\mathbf{h} \in \mathbb{H}^2(\mathbb{R}^2)$ writes (Olive et al., 2018a):

$$\begin{aligned}\mathbf{h} * \mathbf{h} =& (\mathbf{h} \odot \mathbf{h})' \\ =& \mathbf{h} \odot \mathbf{h} - \frac{1}{4}(\mathbf{h} : \mathbf{h})\mathbf{1} \odot \mathbf{1} \\ =& \mathbf{h} \otimes \mathbf{h} - \frac{1}{2}(\mathbf{h} : \mathbf{h})\,\mathbf{J},\end{aligned} \tag{1.1}$$

where

$$\mathbf{J} = \mathbf{I} - \frac{1}{2}\mathbf{1} \otimes \mathbf{1}. \tag{1.2}$$

with $I_{ijkl} = \frac{1}{2}(\delta_{ik}\delta_{jl} + \delta_{il}\delta_{jk})$.

1.4. Covariants of a tensor $\mathbf{T}$ (for the rotation group)

The action $g \star \mathbf{T}$ of a rotation $g \in \mathrm{SO}(d)$ on a tensor $\mathbf{T}$ of order 2 or 4 is

$$(g \star \mathbf{T})_{ij} = g_{ik}g_{jl}T_{kl}, \quad (g \star \mathbf{T})_{ijkl} = g_{ip}g_{jq}g_{kr}g_{ls}T_{pqrs}.$$

A tensor $\mathbf{A}(\mathbf{T})$ is said to be a covariant of tensor $\mathbf{T}$ for $\mathrm{SO}(d)$ if

$$g \star \mathbf{A}(\mathbf{T}) = \mathbf{A}(g \star \mathbf{T}), \quad \forall g \in \mathrm{SO}(d),$$

and dimension d is taken next as $d = 2$.

The algebra of polynomial covariants of the elasticity tensor has been defined (and studied) in (Olive et al., 2018b) for $d = 3$ (three-dimensional case) and in (Desmorat et al., 2020), for $d = 2$ (bi-dimensional case).

2. Harmonic fourth order part H of the 2D elasticity tensor as an harmonic square

2.1. Harmonic decomposition

The harmonic decomposition of tensors is a powerful mathematical tool (Schouten, 1989; Spencer, 1970), that has first been applied to three-dimensional elasticity tensors $\mathbf{C} \in \mathbb{E}\mathrm{la}(\mathbb{R}^3)$ by Backus (1970). Formally in 2D, it is the equivariant decomposition

$$\mathbf{C} = (\mu, \kappa, \mathbf{d}', \mathbf{H}) \in \mathbb{E}\mathrm{la}(\mathbb{R}^2),$$

into two scalars (invariants) $\mu, \kappa \in \mathbb{H}^0(\mathbb{R}^2) \simeq \mathbb{R}$, μ being the shear modulus, κ the bi-dimensional bulk modulus, one harmonic (deviatoric) second order covariant $\mathbf{d}' = \mathbf{d}'(\mathbf{C}) \in \mathbb{H}^2(\mathbb{R}^2)$ and one harmonic fourth order covariant $\mathbf{H} = \mathbf{H}(\mathbf{C}) \in \mathbb{H}^4(\mathbb{R}^2)$, such as

$$g \star \mathbf{C} = (\mu, \kappa, g \star \mathbf{d}', g \star \mathbf{H}) \quad \forall g \in \mathrm{SO}(2).$$

An explicit harmonic decomposition of $\mathbf{C} \in \mathbb{E}\mathrm{la}(\mathbb{R}^2)$ is:

$$\mathbf{C} = 2\mu\mathbf{J} + \kappa\mathbf{1} \otimes \mathbf{1} + \frac{1}{2}(\mathbf{1} \otimes \mathbf{d}' + \mathbf{d}' \otimes \mathbf{1}) + \mathbf{H}, \tag{2.1}$$

with $\mathbf{J}$ defined by (1.2). The closed form expressions of harmonic components μ, κ, $\mathbf{d}'$ and $\mathbf{H}$ are gained thanks to the definition of dilatation and Voigt second order tensors $\mathbf{d} = \mathrm{tr}_{12}\,\mathbf{C}$ and of $\mathbf{v} = \mathrm{tr}_{13}\,\mathbf{C}$,

$$\begin{aligned}\mu =& \frac{1}{8}(2\operatorname{tr}\mathbf{v} - \operatorname{tr}\mathbf{d}), \\ \kappa =& \frac{1}{4}\operatorname{tr}\mathbf{d}, \\ \mathbf{d}' =& \mathbf{d} - \frac{1}{2}(\operatorname{tr}\mathbf{d})\,\mathbf{1}, \\ \mathbf{H} =& \mathbf{C} - 2\mu\mathbf{J} - \kappa\mathbf{1} \otimes \mathbf{1} - \frac{1}{2}(\mathbf{1} \otimes \mathbf{d}' + \mathbf{d}' \otimes \mathbf{1}).\end{aligned} \tag{2.2}$$

In the isotropic (initial) case, one has $\mathbf{H} = 0$ and

$$\mathbf{d} = 2\kappa\mathbf{1}, \qquad \mathbf{v} = (2\mu + \kappa)\mathbf{1},$$

the Young's modulus and Poisson's ratio being

$$E = \frac{4\kappa\mu}{\kappa + \mu}, \qquad \nu = \frac{\kappa - \mu}{\kappa + \mu}.$$

Remark 2.1. In 2D the deviatoric parts of dilatation and of Voigt second order tensors are equal, $\mathbf{v}' = \mathbf{d}'$, and the term $\mathbf{1}\otimes\mathbf{d}' + \mathbf{d}'\otimes\mathbf{1}$ is also equal to $\mathbf{1}\,\underline{\otimes}\,\mathbf{d}' + \mathbf{d}'\,\underline{\otimes}\,\mathbf{1}$, where $(\mathbf{a}\,\underline{\otimes}\,\mathbf{b})_{ij} = \frac{1}{2}(a_{ik}b_{jl} + a_{il}b_{jk})$.

One can also perform the harmonic decomposition of the compliance tensor $\mathbf{S} = \mathbf{C}^{-1}$, and gets then

$$\mathbf{d}'(\mathbf{S}) = \mathbf{v}'(\mathbf{S}) = (\mathrm{tr}_{12}\,\mathbf{S})',$$

where

$$\mathbf{S} = \frac{1}{2\mu}\mathbf{J} + \frac{1}{4\kappa}\mathbf{1}\otimes\mathbf{1} + \frac{1}{2}\left(\mathbf{1}\otimes\mathbf{d}'(\mathbf{S}) + \mathbf{d}'(\mathbf{S})\otimes\mathbf{1}\right) + \mathbf{H}(\mathbf{S}),$$

and $\mathbf{H}(\mathbf{S})$ is the harmonic (totally symmetric and traceless) fourth order part of $\mathbf{S}$.

Recall finally that a minimal generating set (a minimal integrity basis) of the invariant algebra of the elasticity tensor in 2D, under the action of the orthogonal group O(2), consists in the following 5 invariants (Vianello, 1997),

$$\begin{aligned}
\mu &= \frac{1}{8}(2\,\mathrm{tr}\,\mathbf{v} - \mathrm{tr}\,\mathbf{d}),\\
\kappa &= \frac{1}{4}\,\mathrm{tr}\,\mathbf{d},\\
I_2 &= \|\mathbf{d}'\|^2 = \mathbf{d}' : \mathbf{d}',\\
J_2 &= \|\mathbf{H}\|^2 = \mathbf{H} :: \mathbf{H},\\
K_3 &= \mathbf{d} : \mathbf{H} : \mathbf{d}.
\end{aligned} \tag{2.3}$$

2.2. The harmonic part $\mathbf{H} \in \mathbb{H}^4(\mathbb{R}^2)$ as an harmonic square

In 2D, it has been shown that any fourth order harmonic tensor $\mathbf{H} \neq 0$ is of the form (Desmorat and Desmorat, 2015)

$$\mathbf{H} = 2\Lambda\,\mathbf{e}*\mathbf{e}, \quad \mathrm{tr}\,\mathbf{e} = 0, \quad \|\mathbf{e}\| = 1, \tag{2.4}$$

where $\mathbf{e}$ is a unit deviatoric (second order) eigentensor associated with a non zero eigenvalue Λ of the Kelvin representation of $\mathbf{H}$ (*i.e.* such that $\mathbf{H} : \mathbf{e} = \Lambda\mathbf{e}$ in an orthonormal basis).

Remark 2.2. Since $\mathbf{H} \neq 0$ has two opposite eigenvalues $\Lambda_+ > 0$ and $\Lambda_- = -\Lambda_+ < 0$, this implies that any bi-dimensional fourth order harmonic tensor is always an *harmonic square* (Desmorat and Desmorat, 2015, 2016). The corresponding explicit formula is as follows,

$$\mathbf{H} = \mathbf{h} * \mathbf{h}, \qquad \mathbf{h} = \pm\sqrt{2\Lambda_+}\,\mathbf{e}_+, \tag{2.5}$$

where the unit deviatoric second order tensor $\mathbf{e} = \mathbf{e}_+$ is the eigentensor of $\mathbf{H}$ associated with the strictly positive eigenvalue Λ_+. Observe that there are two opposite *harmonic square roots* $\mathbf{h}$ of $\mathbf{H}$, which are opposite to each other. A new proof of this result, more conceptual, is provided in Appendix A.

3. Covariant reconstruction of 2D orthotropic elasticity tensors

Bi-dimensional elasticity tensors $\mathbf{C} \in \mathbb{E}\mathrm{la}(\mathbb{R}^2)$ have Kelvin matrix representation

$$[\mathbf{C}] = \begin{bmatrix} C_{1111} & C_{1122} & \sqrt{2}C_{1112} \\ C_{1122} & C_{2222} & \sqrt{2}C_{1222} \\ \sqrt{2}C_{1112} & \sqrt{2}C_{1222} & 2C_{1212} \end{bmatrix}.$$

Bi-dimensional harmonic fourth order tensors $\mathbf{H} \in \mathbb{H}^4(\mathbb{R}^2)$ have Kelvin representation

$$[\mathbf{H}] = \begin{bmatrix} H_{1111} & -H_{1111} & \sqrt{2}H_{1112} \\ -H_{1111} & H_{1111} & -\sqrt{2}H_{1112} \\ \sqrt{2}H_{1112} & -\sqrt{2}H_{1112} & -2H_{1111} \end{bmatrix}. \tag{3.1}$$

The normal form of an orthotropic elasticity tensor corresponds to $C_{1112} = C_{1222} = 0$. If $\mathbf{C} = \mathbf{H}$ is moreover harmonic, we get $H_{1112} = 0$.

A bi-dimensional harmonic fourth order tensor $\mathbf{H}$ cannot be strictly orthotropic (*i.e.* with exact symmetry group $\mathbb{D}_2$, the symmetry group of a rectangle). A non-vanishing harmonic fourth-order tensor $\mathbf{H}$ has always the symmetry group $\mathbb{D}_4$ (the symmetry group of a square) (Vannucci and Verchery, 2001; Vannucci, 2005). The covariants of $\mathbf{H}$ inherit its symmetry (Olive et al., 2018a,b): this implies that all the second order covariants of $\mathbf{H}$ have at least the square symmetry, they are therefore isotropic (and all the deviatoric second order covariants of $\mathbf{H}$ vanish). Combined with the fact that the harmonic product $*$ is itself covariant, this geometrical property implies that the harmonic square root $\mathbf{h}$ (*i.e.* such as $\mathbf{H} = \mathbf{h} * \mathbf{h}$) is not a covariant of $\mathbf{H}$.

3.1. Square symmetry case

If an elasticity tensor itself has the (exact) *square symmetry*, then $\mathbf{d}' = 0$ and $\mathbf{H} \neq 0$ (Verchery, 1982; Vianello, 1997; Vannucci, 2005), and $\mathbf{C}$ has no better reconstruction formula by means of its covariants than its harmonic decomposition,

$$\mathbf{C} = 2\mu\mathbf{J} + \kappa\mathbf{1}\otimes\mathbf{1} + \mathbf{H}.$$

3.2. Orthotropic case

When an elasticity tensor $\mathbf{C}$ is orthotropic, its second order covariant $\mathbf{d}'$ is an eigentensor of its harmonic part $\mathbf{H} = \mathbf{H}(\mathbf{C})$ (given by (2.1)), *i.e.*

$$\mathbf{H} : \mathbf{d}' = \Lambda\mathbf{d}', \tag{3.2}$$

but where $\Lambda = \pm\Lambda_+$ is a non-vanishing eigenvalue. To check this, just consider its Kelvin normal form

$$[\mathbf{C}] = \begin{bmatrix} C_{1111} & C_{1122} & 0 \\ C_{1122} & C_{2222} & 0 \\ 0 & 0 & 2C_{1212} \end{bmatrix}, \tag{3.3}$$

which leads to

$$\mathbf{d}' = (\mathrm{tr}_{12}\,\mathbf{C})' = \frac{C_{1111} - C_{2222}}{2}\begin{pmatrix}1 & 0\\ 0 & -1\end{pmatrix} \neq 0,$$

and, using (2.1), we get

$$[\mathbf{H}] = H_{1111}\begin{bmatrix}1 & -1 & 0\\ -1 & 1 & 0\\ 0 & 0 & -2\end{bmatrix}.$$

Contracting (3.2) with $\mathbf{d}'$, altogether with the relations

$$\mathbf{H} : \mathbf{1} = \mathbf{1} : \mathbf{H} = 0, \qquad \mathbf{d}' : \mathbf{H} : \mathbf{d}' = K_3,$$

we obtain finally

$$\Lambda = \frac{K_3}{I_2},$$

where the invariants I_2 and K_3 are defined by (2.3). This means by (2.4) that

$$\mathbf{H} = \frac{2\Lambda}{\|\mathbf{d}'\|^2}\mathbf{d}' * \mathbf{d}'.$$

Hence, we have the following result.

Theorem 3.1. *Any bi-dimensional orthotropic elasticity tensor* $\mathbf{C} = (\mu, \kappa, \mathbf{d}', \mathbf{H}) \in \mathbb{E}\mathrm{la}(\mathbb{R}^2)$ *can be reconstructed by means of its 4 invariants* μ, κ, I_2, K_3, *and of its (deviatoric) second order covariant* $\mathbf{d}'$, *as*

$$\begin{aligned}\mathbf{C} =& 2\mu\mathbf{J} + \kappa\mathbf{1}\otimes\mathbf{1} + \frac{1}{2}(\mathbf{1}\otimes\mathbf{d}' + \mathbf{d}'\otimes\mathbf{1}) + \mathbf{H},\\ \mathbf{H} =& \frac{2K_3}{I_2^2}\,\mathbf{d}' * \mathbf{d}',\end{aligned} \tag{3.4}$$

where $\mathbf{d}' * \mathbf{d}' = \mathbf{d}' \otimes \mathbf{d}' - \frac{1}{2}(\mathbf{d}' : \mathbf{d}')\,\mathbf{J}$.

From theorem 3.1, one can derive an upper bound Δ for the distance to orthotropy of a bi-dimensional elasticity tensor as defined below.

Corollary 3.2. *Let* $\mathbf{C} = (\mu, \kappa, \mathbf{d}', \mathbf{H}) \in \mathbb{E}\mathrm{la}(\mathbb{R}^2)$ *be a bi-dimensional elasticity tensor with no material symmetry, let* $I_2 = \|\mathbf{d}'\|^2$, $J_2 = \|\mathbf{H}\|^2$ *and* $K_3 = \mathbf{d} : \mathbf{H} : \mathbf{d}$. *Then, the positive invariant*

$$\begin{aligned}\Delta =& \left\|\mathbf{C} - 2\mu\mathbf{J} - \kappa\mathbf{1}\otimes\mathbf{1} - \frac{1}{2}(\mathbf{1}\otimes\mathbf{d}' + \mathbf{d}'\otimes\mathbf{1}) - \frac{2K_3}{I_2^2}\,\mathbf{d}' * \mathbf{d}'\right\|\\ =& \frac{\sqrt{J_2 I_2^2 - 2K_3^2}}{I_2}.\end{aligned}$$

is an upper bound of the distance of $\mathbf{C}$ *to the orthotropic symmetry class.*

In corollary 3.2, the fact that $\mathbf{C}$ has no material symmetry implies that $\|\mathbf{d}'\|^2 = I_2 \neq 0$. The first equality corresponds to the norm of the difference between the elasticity tensor and its orthotropic reconstruction formula (in which necessarily $\mathbf{d}' \neq 0$). The Harmonic decomposition formula (2.1) gives indeed

$$\Delta = \left\|\mathbf{H} - \frac{2K_3}{I_2^2}\,\mathbf{d}' * \mathbf{d}'\right\|.$$

The second equality in corollary 3.2 is obtained by expanding the square norm, using (1.1) and the facts that $\mathbf{J} :: \mathbf{J} = 2$ and $\mathbf{H} :: \mathbf{J} = 0$, see (Desmorat and Desmorat, 2015).

4. Discrete elements representative volumes

4.1. Beam-particle model

The discrete method used here to perform the virtual testing of a quasi-brittle heterogeneous material is a beam-particle approach detailed in (Vassaux et al., 2016) and summarized in figure 1.

The representative volume is divided into an assembly of rigid particles. The particle mesh is generated from a Voronoi tesselation of a set of randomly generated points within a grid. This operation generates polygonal particles.

Dual of the Voronoi tesselation, the Delaunay triangulation associates a segment with each pair of neighbouring particles. This segment is used as a geometric support for an elastic Euler-Bernoulli beam modelling the cohesion of the material. Each beam b is parameterized by its length l_b, its section A_b, the Young modulus E and the coefficient of inertia $\alpha = 64 I_b \pi / A_b^2$. The first two coefficients l_b and A_b are different for each beam and imposed by the geometry of the mesh. The next two, E and α, are identical for all the beams and identified in order to reproduce the macroscopic elastic behaviour.

In order to reproduce the fracture behaviour, a failure criterion P_{pq} is associated with each beam connecting two particles p and q:

$$P_{pq} = \frac{\varepsilon_{pq}}{\varepsilon_{pq}^{cr}} + \frac{|\theta_p - \theta_q|}{\theta_{pq}^{cr}} > 1 \tag{4.1}$$

where the breaking threshold in extension ε_{pq}^{cr} and the breaking threshold in rotation θ_{pq}^{cr} are generated for each beam according to a Weibull distribution. The Weibull probability density function adopted in this study is :

$$f(x) = \frac{k}{\lambda}\left(\frac{x}{\lambda}\right)^{k-1} e^{-(x/\lambda)^k} \tag{4.2}$$

with the scale factor λ and the shape factor k. In fact, the spatial variability for the two breaking thresholds ε_{pq}^{cr}, θ_{pq}^{cr}, is supposed to be identical. Therefore, three parameters control the fracture behaviour: a shape factor k (common to both distributions), a scale factor in extension $\lambda_{\epsilon_{cr}}$ and a scale factor in rotation $\lambda_{\theta cr}$. The combination of this failure criterion and of a random generation of failure thresholds makes it possible to model a quasi-brittle

behaviour in tension and compression (as proposed and shown in Vassaux et al. (2016)). These three failure parameters are identified in such a way as to reproduce the non-linear behaviour of the material.

Finally, in order to be able to capture the mechanisms of crack closure and of crack sliding, frictional contact is introduced between the particles if they overlap while they are not connected by a beam. The detection of the soft contact between two polygonal particles, the calculation of the normal contact force as well as that of tangential contact via Coulomb's law of friction follows the proposal of Tillemans and Herrmann (1995). A rewriting is however proposed in order to use relative displacements rather than relative velocities (Vassaux et al., 2015b) (figure 1e), the former being more suitable in the quasi-static framework in which we place ourselves. To parametrize the friction, an angle of friction ϕ is introduced resulting in a coefficient of friction $\tan\phi$ for Coulomb's law.

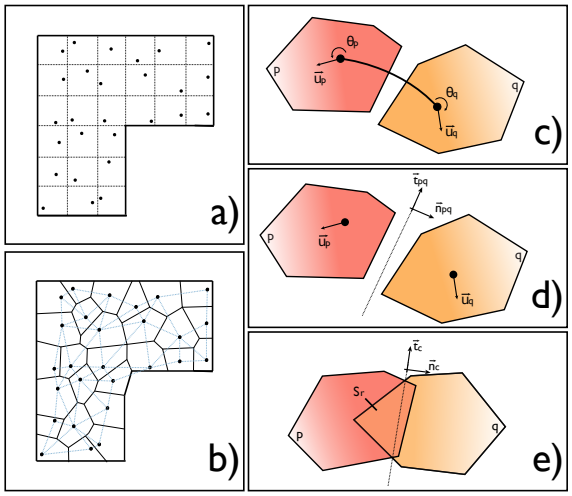

Figure 1: Description of the main ingredients in the beam-particle model (from Oliver-Leblond (2019)).

4.2. Extraction of the effective elasticity tensor

The definition of homogenized quantities on the discrete volume, such as stress and strain, is necessary to link the discrete description, providing detailed information on particle movements and interaction forces, to the continuous description.

The average Cauchy stress tensor is computed from the symmetrization of the definition proposed by Bagi (1996):

$$\boldsymbol{\sigma} = \frac{1}{S}\sum_{p=1}^{N} \mathbf{f}^{(p)} \odot \mathbf{x}^{(p)} \tag{4.3}$$

where S is the area of the discrete representative volume (the so-called Representative Volume Element or RVE in 3D, the Representative Area Element or RAE in 2D), $\mathbf{f}^{(p)}$ is the resulting force on the particle p and $\mathbf{x}^{(p)}$ is the vector position of the center of the particle p. The summation is made on the N particles constituting the boundary of the RAE.

The macroscopic strain tensor is defined as the following mean value:

$$\boldsymbol{\epsilon} = \frac{1}{S}\sum_{p=1}^{N} \left(\frac{\mathbf{u}^{(p)} + \mathbf{u}^{(p+1)}}{2} \odot \boldsymbol{n}^{(p,p+1)} \right) l^{(p,p+1)} \tag{4.4}$$

where $\mathbf{u}^{(p)}$ is the displacement vector of the particle p, $l^{(p,p+1)}$ is the length of the segment linking the particles p and $p+1$ and $\boldsymbol{n}^{(p,p+1)}$ the outward pointing normal vector of this same segment.

In order to obtain the effective elasticity tensor, three measurement loadings are performed and the corresponding average stress and strain vectors are extracted. For each loading i, the effective elasticity tensor links the stress to the strain in the following way:

$$\hat{\sigma}^{(i)} = [\mathbf{C}]\,\hat{\epsilon}^{(i)} \tag{4.5}$$

where $[\mathbf{C}]$ is Kelvin matrix representation of macroscopic elasticity tensor $\mathbf{C}$ and

$$\hat{\sigma}^{(i)} = \begin{pmatrix} \sigma_{11}^{(i)} \\ \sigma_{22}^{(i)} \\ \sqrt{2}\sigma_{12}^{(i)} \end{pmatrix}, \quad \hat{\epsilon}^{(i)} = \begin{pmatrix} \epsilon_{11}^{(i)} \\ \epsilon_{22}^{(i)} \\ \sqrt{2}\epsilon_{12}^{(i)} \end{pmatrix}.$$

Therefore, if the measurement loadings are chosen to ensure that the strain vectors are linearly independent, their determinant is non-zero and the symmetric effective elasticity tensor can be computed from

$$[\mathbf{C}] = \left(\left(\hat{\sigma}^{(1)}\ \hat{\sigma}^{(2)}\ \hat{\sigma}^{(3)} \right) \left(\hat{\epsilon}^{(1)}\ \hat{\epsilon}^{(2)}\ \hat{\epsilon}^{(3)} \right)^{-1} \right)^{s}. \tag{4.6}$$

4.3. Definition of possible measurement loadings

Two requirements must be met to define the measurement loadings: ensuring the linear independence of the strain vectors and maintaining the cracks open during measurement. Several sets of measurement loadings are used and compared:

- DEF_WoC : Elementary strain loading without contact

$$\hat{\epsilon}^{(1)} = \begin{pmatrix} \epsilon \\ 0 \\ 0 \end{pmatrix}, \quad \hat{\epsilon}^{(2)} = \begin{pmatrix} 0 \\ \epsilon \\ 0 \end{pmatrix}, \quad \hat{\epsilon}^{(3)} = \begin{pmatrix} 0 \\ 0 \\ \sqrt{2}\epsilon \end{pmatrix},$$

  where ϵ is the applied strain that must be sufficiently small for the (possibly cracked) RAE to remain in the elasticity domain. The following displacement fields are thus applied on the boundaries of the specimen:

$$\mathbf{u}^{(1)} = \begin{pmatrix} \epsilon x \\ 0 \end{pmatrix}, \quad \mathbf{u}^{(2)} = \begin{pmatrix} 0 \\ \epsilon y \end{pmatrix}, \quad \mathbf{u}^{(3)} = \begin{pmatrix} \epsilon y \\ \epsilon x \end{pmatrix},$$

  with x and y the positions of the center of the particles on the boundaries.

- DEF_BT_C : Bi-tension strain loading with contact

$$\hat{\epsilon}^{(1)} = \begin{pmatrix} \epsilon_{bt} + \epsilon \\ \epsilon_{bt} \\ 0 \end{pmatrix}, \quad \hat{\epsilon}^{(2)} = \begin{pmatrix} \epsilon_{bt} \\ \epsilon_{bt} + \epsilon \\ 0 \end{pmatrix}, \quad \hat{\epsilon}^{(3)} = \begin{pmatrix} \epsilon_{bt} \\ \epsilon_{bt} \\ \sqrt{2}\epsilon \end{pmatrix},$$

where ϵ_{bt} is introduced to create a bi-tension loading keeping the cracks open. The following displacement fields are thus applied on the boundaries of the specimen:

$$\mathbf{u}^{(1)} = \begin{pmatrix} (\epsilon_{bt} + \epsilon)x \\ \epsilon_{bt} y \end{pmatrix}, \quad \mathbf{u}^{(2)} = \begin{pmatrix} \epsilon_{bt} x \\ (\epsilon_{bt} + \epsilon)y \end{pmatrix}, \quad \mathbf{u}^{(3)} = \begin{pmatrix} \epsilon_{bt} x + \epsilon y \\ \epsilon x + \epsilon_{bt} y \end{pmatrix},$$

- SIG_F_WoC : Elementary stress loading with applied forces without contact

$$\hat{\sigma}^{(1)} = \begin{pmatrix} \sigma \\ 0 \\ 0 \end{pmatrix}, \quad \hat{\sigma}^{(2)} = \begin{pmatrix} 0 \\ \sigma \\ 0 \end{pmatrix}, \quad \hat{\sigma}^{(3)} = \begin{pmatrix} 0 \\ 0 \\ \sqrt{2}\sigma \end{pmatrix},$$

where σ is the applied stress that must be sufficiently small to remain in the elasticity domain. The traction vectors $\mathbf{t} = \boldsymbol{\sigma}\mathbf{n}$ are then applied on the boundaries ($\mathbf{n}$: outer unit normal) and the central particle is completely blocked to avoid rigid motions:

$$\mathbf{t}^{(1)}_{xmin} = \begin{pmatrix} -\sigma \\ 0 \end{pmatrix}, \quad \mathbf{t}^{(1)}_{xmax} = \begin{pmatrix} \sigma \\ 0 \end{pmatrix},$$

$$\mathbf{t}^{(2)}_{ymin} = \begin{pmatrix} 0 \\ -\sigma \end{pmatrix}, \quad \mathbf{t}^{(2)}_{ymax} = \begin{pmatrix} 0 \\ \sigma \end{pmatrix},$$

$$\mathbf{t}^{(3)}_{xmin} = \begin{pmatrix} 0 \\ -\sigma \end{pmatrix}, \quad \mathbf{t}^{(3)}_{xmax} = \begin{pmatrix} 0 \\ \sigma \end{pmatrix}, \quad \mathbf{t}^{(3)}_{ymin} = \begin{pmatrix} -\sigma \\ 0 \end{pmatrix}, \quad \mathbf{t}^{(3)}_{ymax} = \begin{pmatrix} \sigma \\ 0 \end{pmatrix}.$$

- SIG_D_WoC : Elementary stress loading with applied displacements without contact.

The objective is to obtain the three stress states of the previous measurement loading by applying only kinematic conditions.

$$\mathbf{u}^{(1)}_{xmin} \cdot \boldsymbol{e}_x = 0, \quad \mathbf{u}^{(1)}_{xmax} \cdot \boldsymbol{e}_x = u, \quad \mathbf{u}^{(1)}_{ymin} \cdot \boldsymbol{e}_y = 0,$$

$$\mathbf{u}^{(2)}_{ymin} \cdot \boldsymbol{e}_y = 0, \quad \mathbf{u}^{(2)}_{ymax} \cdot \boldsymbol{e}_y = u, \quad \mathbf{u}^{(2)}_{xmin} \cdot \boldsymbol{e}_x = 0,$$

$$\mathbf{u}^{(3)}_{xmin} \cdot \boldsymbol{e}_y = 0, \quad \mathbf{u}^{(3)}_{xmax} \cdot \boldsymbol{e}_y = \sqrt{2}u, \quad \mathbf{u}^{(3)}_{ymin} \cdot \boldsymbol{e}_x = 0, \quad \mathbf{u}^{(3)}_{ymax} \cdot \boldsymbol{e}_x = \sqrt{2}u.$$

where $\mathbf{u}$ is the applied displacement that must be sufficiently small for the RAE to remain in the elasticity domain.

4.4. Comparison of the different measurement loadings

We first compare the four measurement loadings described previously on an uncracked square specimen of 100×100 particles (see first line of table 1). We observe that they give very close results. The dispersion can be attributed to the measurement noise. This result was expected because there are enough particles in the specimen to make it a Representative Area Element. Thus, the type of boundary conditions does not influence the result, as in an infinite medium.

Measurements of the effective elasticity tensors of cracked specimens are a more important feature of the present study. For this purpose, two cracking tests are carried out: a localized cracking test and a diffuse cracking test. In both cases, the orientation of the loads is such that the micro-cracks are globally perpendicular to the y direction. For each type of cracking, we extract the crack patterns and the associated effective elasticity tensors for three levels of damage D (computed as a relative loss of stiffness in the y direction, Lemaitre and Chaboche (1985)): a low level of damage ($D \approx 0.1$), a mid level of damage ($D \approx 0.4$) and a high level of damage ($D \approx 0.7$) as presented in table 1. The goal here is then to compare the four measurement loadings in order to select one of them for the rest of the study.

Regardless of the type or amount of cracking, the two strain loads (DEF_WoC and DEF_BT_C) give similar results. This is expected and confirms that it is sufficient to deactivate the contact within the discrete model in order to obtain a measurement loading equivalent to a loading keeping the cracks open. Since the strain loading with additional bi-tension (DEF_BT_C) can cause convergence problems, it is important to be able to validate this equivalence with the elementary strain loading where the contact is deactivated (DEF_WoC).

In the same way, we can observe that the two elementary stress loadings (SIG_F_WoC and SIG_D_WoC) give identical results, up to the measurement noise, whether forces or displacements are applied on the boundaries. Although this was not the case here, stress loading with applied forces may prove to be less robust because the blocking of the central particle, to prevent rigid body movements, can lead to convergence problems if this particle is in an area of significant cracking.

Finally, strain and stress loadings give identical results in the case of diffuse cracking even for a significant level of damage. On the other hand, the results diverge for the case of localized cracking (see figure 2). Indeed, if we pursue the simulation until the complete failure of the specimen in the localized case, we notice that the C_{2222} modulus approaches 0 for the measurement loading in stress, which is not the case for the measurement loading in strain. Here, we encounter a limitation in the use of damage models for quasi-brittle materials such as concrete. Indeed, the damage is intended to represent diffuse cracking and is thus not appropriate for cases of localized cracking. However,

Crack patterns	DEF_WoC	DEF_BT_C	SIG_F_WoC	SIG_D_WoC
Initial state No damage 	$\begin{bmatrix} 38.3 & 8.1 & 0.1 \\ 8.1 & 38.4 & -0.3 \\ 0.1 & -0.3 & 29.2 \end{bmatrix}$	$\begin{bmatrix} 38.4 & 8.0 & -0.3 \\ 8.0 & 38.6 & -0.1 \\ -0.3 & -0.1 & 29.4 \end{bmatrix}$	$\begin{bmatrix} 38.0 & 8.1 & 0.1 \\ 8.1 & 38.6 & 0.0 \\ 0.1 & 0.0 & 29.4 \end{bmatrix}$	$\begin{bmatrix} 38.3 & 8.1 & 0.1 \\ 8.1 & 38.4 & -0.1 \\ 0.1 & -0.1 & 29.2 \end{bmatrix}$
Localized cracking Low level of damage 	$\begin{bmatrix} 38.1 & 7.4 & 0.0 \\ 7.4 & 34.6 & -0.4 \\ 0.0 & -0.4 & 28.6 \end{bmatrix}$	$\begin{bmatrix} 38.2 & 7.3 & -0.3 \\ 7.3 & 34.7 & -0.4 \\ -0.3 & -0.4 & 28.6 \end{bmatrix}$	$\begin{bmatrix} 37.7 & 7.4 & 0.0 \\ 7.4 & 34.4 & -0.3 \\ 0.0 & -0.3 & 28.6 \end{bmatrix}$	$\begin{bmatrix} 38.0 & 7.3 & 0.0 \\ 7.3 & 34.1 & -0.4 \\ 0.0 & -0.4 & 28.2 \end{bmatrix}$
Localized cracking Mid level of damage 	$\begin{bmatrix} 37.6 & 5.6 & 0.4 \\ 5.6 & 25.6 & 1.1 \\ 0.4 & 1.1 & 27.2 \end{bmatrix}$	$\begin{bmatrix} 37.7 & 5.5 & 0.0 \\ 5.5 & 25.8 & 1.3 \\ 0.0 & 1.3 & 27.2 \end{bmatrix}$	$\begin{bmatrix} 37.2 & 5.0 & 0.4 \\ 5.0 & 23.0 & 1.6 \\ 0.4 & 1.6 & 26.6 \end{bmatrix}$	$\begin{bmatrix} 37.5 & 5.0 & 0.4 \\ 5.0 & 22.7 & 1.6 \\ 0.4 & 1.6 & 26.4 \end{bmatrix}$
Localized cracking High level of damage 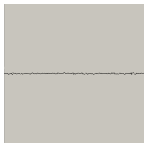	$\begin{bmatrix} 37.2 & 3.7 & -0.3 \\ 3.7 & 17.0 & -1.6 \\ -0.3 & -1.6 & 24.0 \end{bmatrix}$	$\begin{bmatrix} 37.3 & 3.6 & -0.7 \\ 3.6 & 17.1 & -1.4 \\ -0.7 & -1.4 & 24.2 \end{bmatrix}$	$\begin{bmatrix} 36.6 & 2.6 & -0.7 \\ 2.6 & 12.0 & -2.1 \\ -0.7 & -2.1 & 21.4 \end{bmatrix}$	$\begin{bmatrix} 36.9 & 2.5 & -0.4 \\ 2.5 & 11.9 & -2.1 \\ -0.4 & -2.1 & 21.4 \end{bmatrix}$
Diffused cracking Low level of damage 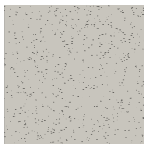	$\begin{bmatrix} 38.2 & 8.0 & 0.1 \\ 8.0 & 34.4 & -0.3 \\ 0.1 & -0.3 & 28.4 \end{bmatrix}$	$\begin{bmatrix} 38.3 & 7.9 & -0.3 \\ 7.9 & 34.5 & -0.1 \\ -0.3 & -0.1 & 28.6 \end{bmatrix}$	$\begin{bmatrix} 37.8 & 8.0 & 0.1 \\ 8.0 & 34.2 & 0.0 \\ 0.1 & 0.0 & 28.4 \end{bmatrix}$	$\begin{bmatrix} 38.1 & 8.0 & 0.1 \\ 8.0 & 34.1 & -0.3 \\ 0.1 & -0.3 & 28.2 \end{bmatrix}$
Diffused cracking Mid level of damage 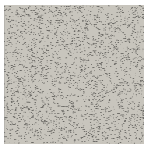	$\begin{bmatrix} 37.7 & 7.4 & 0.1 \\ 7.4 & 23.5 & -0.3 \\ 0.1 & -0.3 & 24.6 \end{bmatrix}$	$\begin{bmatrix} 37.8 & 7.3 & -0.3 \\ 7.3 & 23.6 & -0.1 \\ -0.3 & -0.1 & 24.8 \end{bmatrix}$	$\begin{bmatrix} 37.2 & 7.3 & 0.1 \\ 7.3 & 23.0 & -0.1 \\ 0.1 & -0.1 & 24.6 \end{bmatrix}$	$\begin{bmatrix} 37.6 & 7.3 & 0.1 \\ 7.3 & 23.0 & -0.1 \\ 0.1 & -0.1 & 24.4 \end{bmatrix}$
Diffused cracking High level of damage 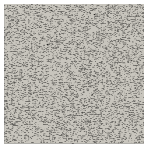	$\begin{bmatrix} 36.2 & 6.3 & 0.1 \\ 6.3 & 12.5 & 0.1 \\ 0.1 & 0.1 & 18.6 \end{bmatrix}$	not converged	$\begin{bmatrix} 35.6 & 5.8 & 0.1 \\ 5.8 & 11.7 & 0.1 \\ 0.1 & 0.1 & 18.2 \end{bmatrix}$	$\begin{bmatrix} 36.2 & 6.1 & 0.3 \\ 6.1 & 12.0 & 0.1 \\ 0.3 & 0.1 & 18.2 \end{bmatrix}$

Table 1: Comparison of the measurement loadings used to extract the effective elasticity tensor [**C**] (in GPa, Kelvin representation).

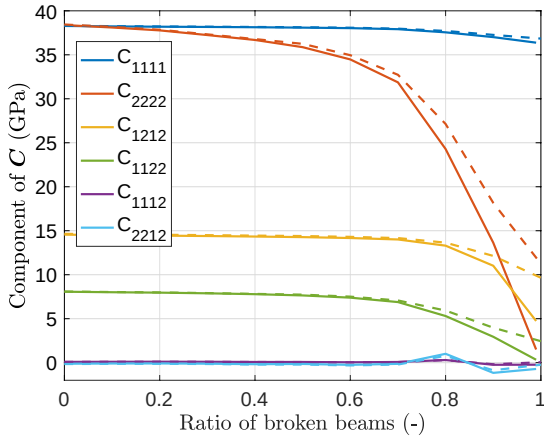

Figure 2: Evolution of the components of the effective elasticity tensor for the localized cracking test according to the elementary strain loading measurement (DEF_WoC in dashed lines) and the elementary stress loading measurement with applied displacements (SIG_D_WoC in plain lines)

damage models are commonly used up to high levels of degradation, where the cracks are almost necessarily localized in a quasi-brittle material. In order to correctly represent the loss of stiffness due to this localized cracking while keeping the simplicity of a kinematic loading, we decide to choose thereafter the elementary stress loading with applied displacements without contact (SIG_D_WoC).

5. Deviation from isotropy of the initial tensor

5.1. Geometrical isotropy

The isotropy of discrete media is generally studied from a geometric point of view (André et al., 2012). Indeed, the geometrical isotropy of the mesh is considered as a good criterion to approach the mechanical isotropy of the material if the elasticity parameters are homogeneous over the domain. This geometric isotropy can be visualized simply by plotting the polar histogram associated with the orientation of the beams. The figure 3 presents those polar histograms for three meshes of different densities. One can see that the polar histogram tends towards a circle as the density increases, which shows geometrical isotropy convergence.

5.2. Mechanical isotropy

Through the harmonic decomposition of the elasticity tensors of each material samples, it is possible to quantify their deviation from isotropy. The evaluation of the relative distance of the elasticity tensors to the isotropic class thus provides a criterion for quantifying the validity of the mechanical isotropy hypothesis.

Figure 4 presents the evolution with the mesh size of the relative distance to isotropy Δ_{iso} defined as :

$$\Delta_{iso} = \frac{\|\mathbf{C} - \mathbf{C}_{iso}\|}{\|\mathbf{C}\|} \tag{5.1}$$

with $\mathbf{C}_{iso} = 2\mu\mathbf{J} + \kappa\mathbf{1}\otimes\mathbf{1}$ the isotropic projection of $\mathbf{C}$. The elasticity parameters μ and κ are determined by Eq. (2.2).

For each mesh density, several simulations have been performed (from 200 simulations for the 10×10 particles mesh to 50 simulations for a 300×300 particles mesh). As expected, the assumption of an initial isotropic medium is correct if the number of particles is sufficient. In Figure 3, the elasticity tensors obtained for three simulations are given along with the associated isotropic tensors and elasticity coefficients.

Given the above results, it seems safe to adopt a mesh density of 100×100 particles to ensure the mechanical isotropy of the initial, uncracked, state.

6. Multiaxial analyses of effective elasticity tensors up to high level of damage

In this part, a 20cm×20cm specimen representative of mortar is subjected to various loads. As mentioned before, the simulation is done with 100×100 particles, which results in an average beam size $\overline{l_b}$ of 2 mm.

The parameters of the discrete model, given in the table 2, are chosen so as to reproduce macroscopically the behaviour of a mortar of Young's modulus $E = 36.35$ GPa and Poisson ratio $\nu = 0.22$ (corresponding to $\kappa = 23.24$ GPa and $\mu = 14.92$ GPa), of tensile strength $f_t = 3$ MPa and of compressive strength $f_c = 40$ Mpa.

Symbol	Values	Unit
$\overline{l_b}$	2	mm
E_b	46	GPa
α	0.83	-
$\lambda_{\epsilon_{cr}}$	$2.4\ 10^{-4}$	-
$\lambda_{\theta_{cr}}$	$3.3\ 10^{-3}$	-
k	2.8	-
$\tan\phi$	0.7	-

Table 2: Numerical parameters for the beam-particle model.

6.1. Studied loadings

The loadings are chosen so as to obtain different cracking paths:

- Tension along the y-axis (see figure 5);
- Compression along the y-axis with unrestrained boundary conditions along the x-axis (see figure 6);
- Bi-tension along the x-axis and y-axis (see figure 7);
- Simple shear (see figure 8);

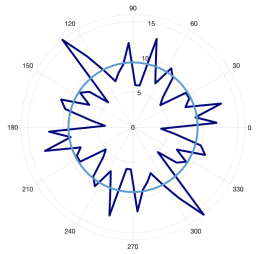
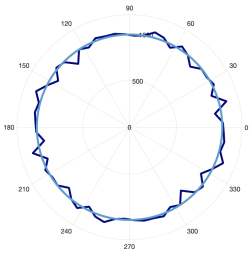
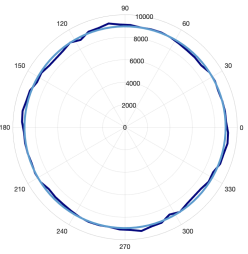

$$[\mathbf{C}] = \begin{bmatrix} 43.13 & 8.42 & -0.81 \\ 8.42 & 42.65 & 0.48 \\ -0.81 & 0.48 & 30.62 \end{bmatrix} \qquad [\mathbf{C}] = \begin{bmatrix} 38.72 & 7.90 & -0.24 \\ 7.90 & 38.44 & -0.10 \\ -0.24 & -0.10 & 29.00 \end{bmatrix} \qquad [\mathbf{C}] = \begin{bmatrix} 38.06 & 8.09 & 0.00 \\ 8.09 & 38.07 & -0.03 \\ 0.00 & -0.03 & 29.00 \end{bmatrix}$$

$$[\mathbf{C}_{iso}] = \begin{bmatrix} 41.92 & 9.39 & 0.00 \\ 9.39 & 41.92 & 0.00 \\ 0.00 & 0.00 & 32.54 \end{bmatrix} \qquad [\mathbf{C}_{iso}] = \begin{bmatrix} 38.16 & 8.32 & 0.00 \\ 8.32 & 38.16 & 0.00 \\ 0.00 & 0.00 & 29.84 \end{bmatrix} \qquad [\mathbf{C}_{iso}] = \begin{bmatrix} 37.82 & 8.34 & 0.00 \\ 8.34 & 37.82 & 0.00 \\ 0.00 & 0.00 & 29.48 \end{bmatrix}$$

$\kappa = 25.65$ GPa, $\mu = 16.27$ Gpa
$E = 38.82$ GPa, $\nu = 0.22$

(a) 10×10

$\kappa = 23.24$ GPa, $\mu = 14.92$ Gpa
$E = 36.35$ GPa, $\nu = 0.22$

(b) 100×100

$\kappa = 23.08$ GPa, $\mu = 14.74$ Gpa
$E = 35.98$ GPa, $\nu = 0.22$

(c) 300×300

Figure 3: Polar histograms of the beams orientation for different mesh densities, elasticity tensors and associated isotropic tensors (in GPa, Kelvin representation).

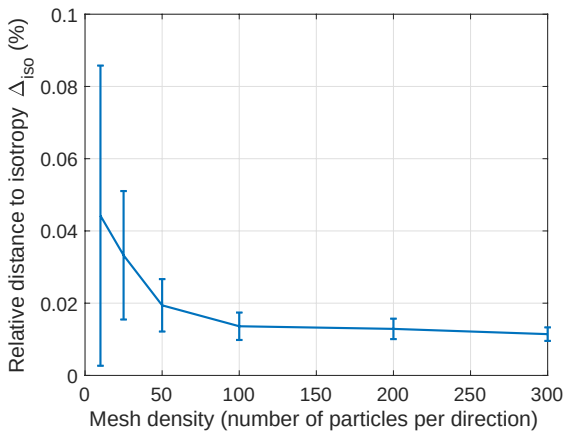

Figure 4: Evolution of the relative distance to isotropy (5.1) with the mesh density.

- Willam loading (Willam et al., 1989) consisting on a simple tension along the y-axis pursued up to the tensile stress followed by a combination of bi-tension and shear with an increase of the strain components ϵ_{xx}, ϵ_{yy} and ϵ_{xy} in the proportions 1.5/1.0/0.5 (see figure 9). This numerical test was proposed to induce a rotation of the principal stress/strain directions leading to a misalignment with the material axes of orthotropy associated with the initial crack direction.

For each of them, we first observe a development of diffuse micro-cracks and then a localization of these micro-cracks leading to the propagation of the macro-crack.

In order to follow the breakage of the specimen, the evolution of the ratio of broken beams is plotted in comparison with the macroscopic response. This ratio is initially worth 0, when the specimen is intact, and reaches 1 at the end of loading when the specimen can no longer sustain any effort. The total number of broken beams is usually far from the number of beams in the specimen.

We can notice snap-back phenomena in the evolution curves of the ratio of broken beams. These snap-backs are related to avalanche breakage phenomena (Rinaldi and Lai, 2007), classical for lattice simulations of quasi-brittle materials, and are visible in the complete macroscopic responses (see figure 5). These macroscopic responses are smoothed on the figures 5 to 9 to get closer to the type of data observed experimentally. However, the extraction of the effective elasticity tensors is not impacted by this post-treatment of the curves.

These loadings allow us to quantify the impact on the

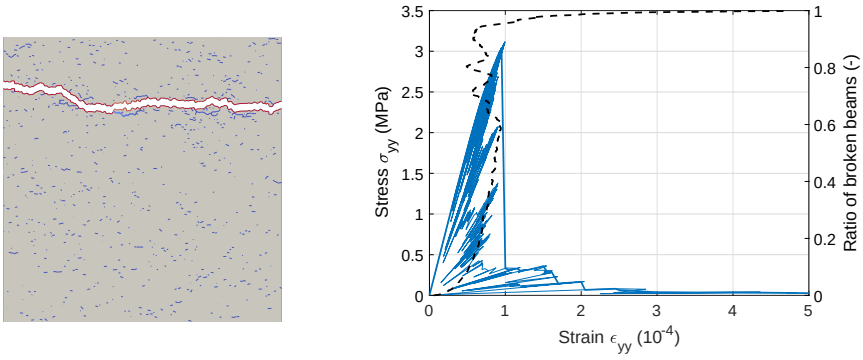

Figure 5: Tensile loading: final crack pattern, macroscopic responses (complete and smoothed) and evolution of the ratio of broken beams (dashed line).

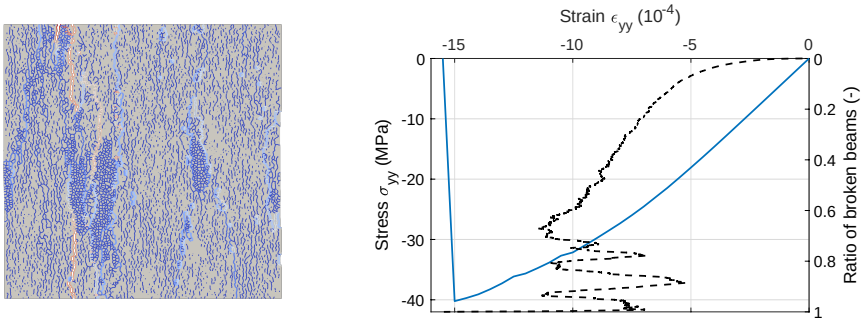

Figure 6: Compressive loading: final crack pattern, macroscopic response and evolution of the ratio of broken beams (dashed line).

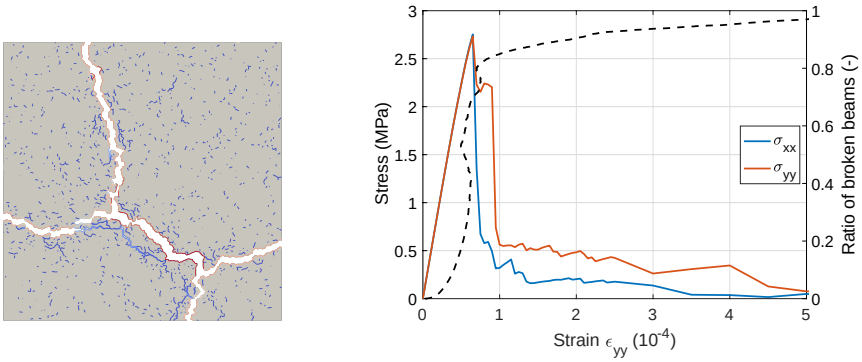

Figure 7: Bi-Tensile loading: final crack pattern, macroscopic response and evolution of the ratio of broken beams (dashed line).

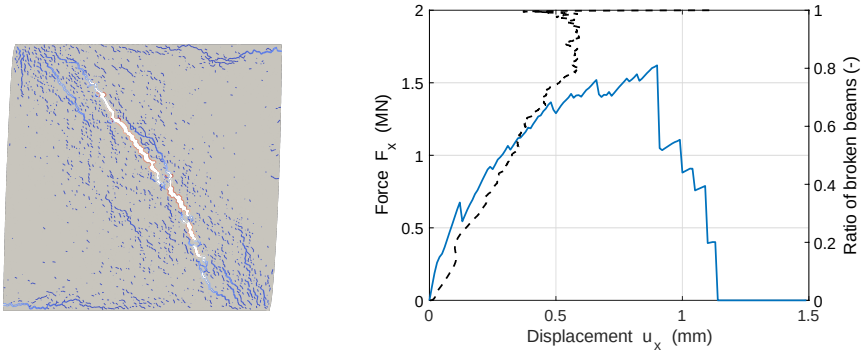

Figure 8: Simple shear loading: final crack pattern, macroscopic response and evolution of the ratio of broken beams (dashed line).

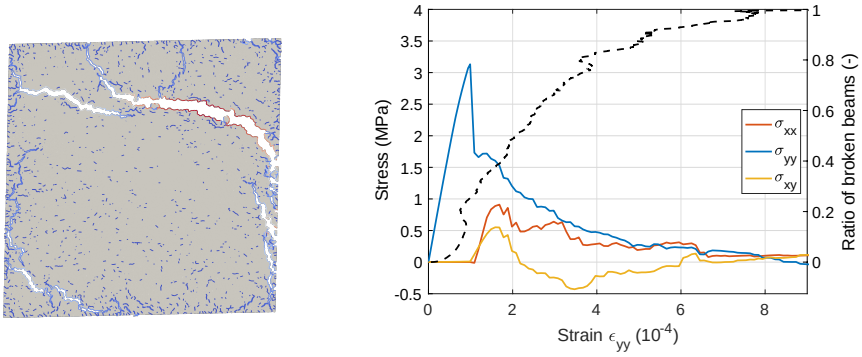

Figure 9: Willam loading: final crack pattern, macroscopic response and evolution of the ratio of broken beams (dashed line).

effective (damaged) elasticity tensor of the presence of micro-cracks in different directions, which may nucleate or rotate.

6.2. Orthotropy of the effective stiffness tensors

For the previously defined loadings, the stiffness and compliance tensors were extracted at different ratio of broken beams. The evolution of Δ, which is an upper bound of the distance to the orthotropic class for an elasticity tensor as defined in corollary 3.2, is plotted in the figures 10 and 11. It should be noted that it is not always possible to extract the elasticity tensors for very high levels of damage.

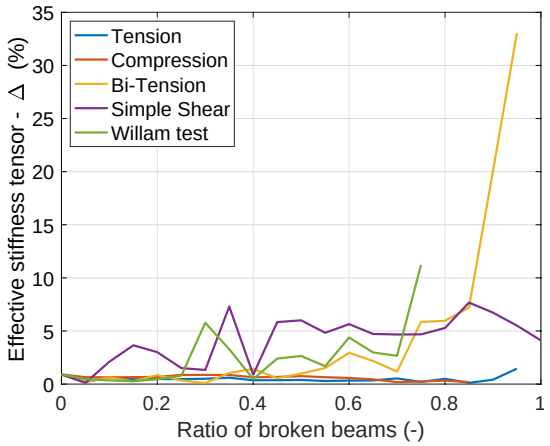

Figure 10: Upper-bound of distance to orthotropy for the effective stiffness tensors

Even at high levels of damage, the elasticity tensors remain close to the orthotropic symmetry class. This is even truer in the case of the compliance tensors. It is interesting to note that in the case of Willam loading, which results in a non-orthotropic cracking pattern, the deviations from orthotropy remain small. The largest deviation observed corresponds to the case of the stiffness tensor for bi-tension loading. This may be related to the coalescence of the main two orthogonal cracks.

One should note that the orthotropy of the effective elasticity tensor $\tilde{\mathbf{C}} = \tilde{\mathbf{S}}^{-1}$ is a sufficient condition to define an orthotropic damage tensor (see next), since the initial elasticity tensor $\mathbf{C} = \mathbf{S}^{-1}$ is isotropic.

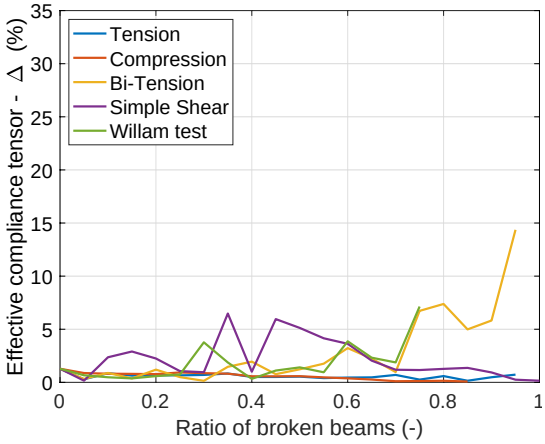

Figure 11: Upper-bound of distance to orthotropy for the effective compliance tensors

6.3. Comparison with micromechanics of cracked solids

In the bi-dimensional micromechanical approach summarized by Kachanov (1992), the material is considered to be initially isotropic with an initial (undamaged) compliance tensor,

$$\mathbf{S} = \frac{1}{2\mu}\mathbf{J} + \frac{1}{4\kappa}\mathbf{1}\otimes\mathbf{1}. \tag{6.1}$$

Damage is introduced using several networks of cracks with no interactions between each other. A family of cracks p is characterized by its orientation $\boldsymbol{n}^{(p)}$, which is the normal to all the cracks in this family, a length $2l^{(p)}$ and a density of micro-cracks $\omega^{(p)} = \pi l^{(p)}/A$ with A the area of the RAE.

A crack density tensor is then introduced for the network of all the families of cracks:

$$\boldsymbol{\omega} = \sum_p \omega^{(p)} \boldsymbol{n}^{(p)} \otimes \boldsymbol{n}^{(p)} \tag{6.2}$$

Gibbs free enthalpy density of the cracked solid writes,

in case of open cracks (Kachanov, 1992):

$$\begin{aligned}\rho\psi^\star &= \frac{1}{2}\boldsymbol{\sigma} : \tilde{\mathbf{S}} : \boldsymbol{\sigma} \\ &= \frac{1}{2}\boldsymbol{\sigma} : \mathbf{S} : \boldsymbol{\sigma} + \frac{1}{E}\,\mathrm{tr}\,(\boldsymbol{\sigma}\cdot\boldsymbol{\omega}\cdot\boldsymbol{\sigma}) \\ &= \frac{1}{2}\boldsymbol{\sigma} : \mathbf{S} : \boldsymbol{\sigma} + \frac{1}{2E}\,\boldsymbol{\sigma} : (\mathbf{1}\,\overline{\otimes}\,\boldsymbol{\omega} + \boldsymbol{\omega}\,\overline{\otimes}\,\mathbf{1}) : \boldsymbol{\sigma}\end{aligned} \tag{6.3}$$

with $\mathbf{S}$ the initial (isotropic) compliance tensor (E being the Young modulus of the isotropic uncracked solid) and where $\tilde{\mathbf{S}}$ is the effective compliance tensor.

We recall here the harmonic decomposition of the compliance tensor (see remark 2.1):

$$\begin{aligned}\tilde{\mathbf{S}} &= \tilde{\mathbf{S}}_{iso} + \frac{1}{2}\left(\mathbf{1}\otimes\mathbf{d}'(\tilde{\mathbf{S}}) + \mathbf{d}'(\tilde{\mathbf{S}})\otimes\mathbf{1}\right) + \mathbf{H}(\tilde{\mathbf{S}}) \\ &= \tilde{\mathbf{S}}_{iso} + \frac{1}{2}\left(\mathbf{1}\,\overline{\otimes}\,\mathbf{d}'(\tilde{\mathbf{S}}) + \mathbf{d}'(\tilde{\mathbf{S}})\,\overline{\otimes}\,\mathbf{1}\right) + \mathbf{H}(\tilde{\mathbf{S}})\end{aligned} \tag{6.4}$$

with $\mathbf{d}(\tilde{\mathbf{S}}) = \mathrm{tr}_{12}\,\tilde{\mathbf{S}}$ (in the same way $\mathbf{v}(\tilde{\mathbf{S}}) = \mathrm{tr}_{13}\,\tilde{\mathbf{S}}$) and where (see Eq. (2.2))

$$\tilde{\mathbf{S}}_{iso} = \frac{1}{2\tilde{\mu}}\mathbf{J} + \frac{1}{4\tilde{\kappa}}\mathbf{1}\otimes\mathbf{1}, \quad \begin{cases}\frac{1}{2\tilde{\mu}} = \frac{1}{4}(2\,\mathrm{tr}\,\mathbf{v}(\tilde{\mathbf{S}}) - \mathrm{tr}\,\mathbf{d}(\tilde{\mathbf{S}})),\\ \frac{1}{4\tilde{\kappa}} = \frac{1}{4}\,\mathrm{tr}\,\mathbf{d}(\tilde{\mathbf{S}}).\end{cases}$$

By comparing equations (6.3) and (6.4), it can be concluded that in the case of Kachanov micro-cracking theory (representing networks of non interacting open micro-cracks), one has $\tilde{\mathbf{S}}_{iso} = \mathbf{S} + \frac{1}{2E}\,\mathrm{tr}\boldsymbol{\omega}\,\mathbf{1}\,\overline{\otimes}\,\mathbf{1}$ (with $\mathbf{1}\,\overline{\otimes}\,\mathbf{1} = \mathbf{I} = \mathbf{J} + \frac{1}{2}\mathbf{1}\otimes\mathbf{1}$), $\mathbf{d}'(\mathbf{S}) = 2\boldsymbol{\omega}'/E$ and the harmonic part of the compliance tensor $\mathbf{H}(\tilde{\mathbf{S}})$ vanishes.

In order to test the validity of the property $\mathbf{H}(\tilde{\mathbf{S}}) = 0$, eventually when cracks interaction takes place, we plot in figures 12 to 16 the evolution of the three parts of the effective compliance tensor $\tilde{\mathbf{S}}$ (computed thanks to the beam-particle method):

- the isotropic part $\tilde{\mathbf{S}}_{iso}$,
- the deviatoric dilatation part $\frac{1}{2}(\mathbf{1}\otimes\mathbf{d}'(\tilde{\mathbf{S}})+\mathbf{d}'(\tilde{\mathbf{S}})\otimes\mathbf{1})$,
- and the harmonic part $\mathbf{H}(\tilde{\mathbf{S}})$,

according to the ratio of broken beams. One should remember that the deviatoric dilatation part is always orthotropic while the harmonic part can have the square symmetry or be zero.

With these curves, we can distinguish four stages of cracking:

i) Initially, the medium is non-cracked and therefore isotropic, which implies that the parts related to $\mathbf{d}'$ and $\mathbf{H}$ are null.

ii) At the beginning of loading, only the weakest beams break without influence of the loading direction. The orientation of the cracks therefore remains isotropic and here again the parts linked to $\mathbf{d}'$ and $\mathbf{H}$ are zero.

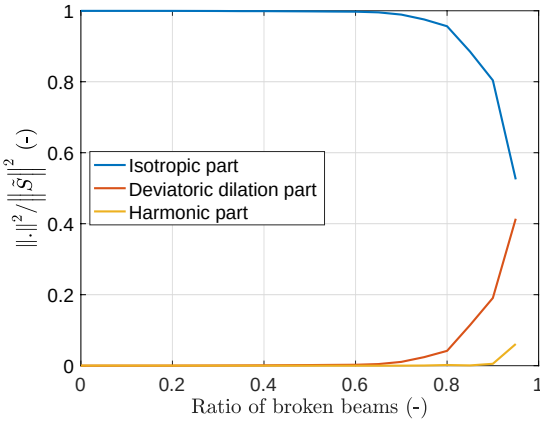

Figure 12: Tensile loading: Evolution of the relative parts of the effective compliance tensor with the ratio of broken beams.

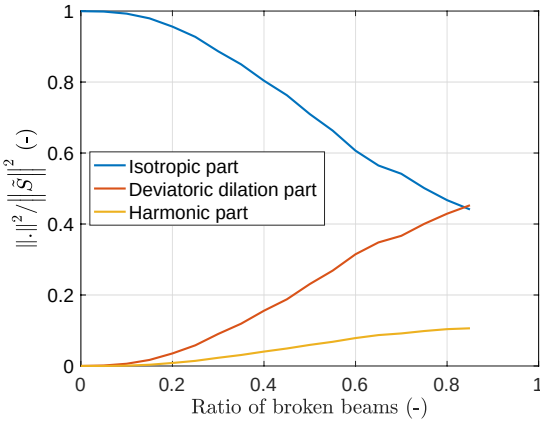

Figure 13: Compressive loading: Evolution of the relative parts of the effective compliance tensor with the ratio of broken beams.

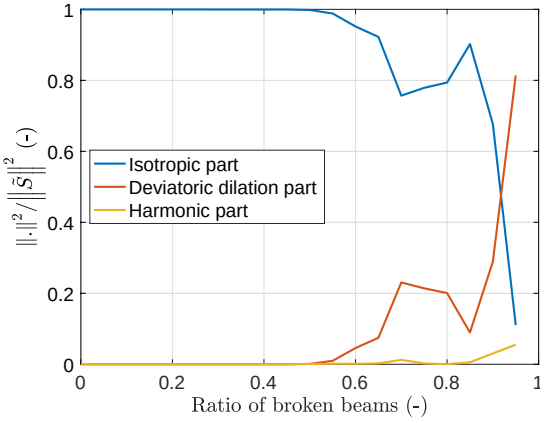

Figure 14: Bi-Tensile loading: Evolution of the relative parts of the effective compliance tensor with the ratio of broken beams.

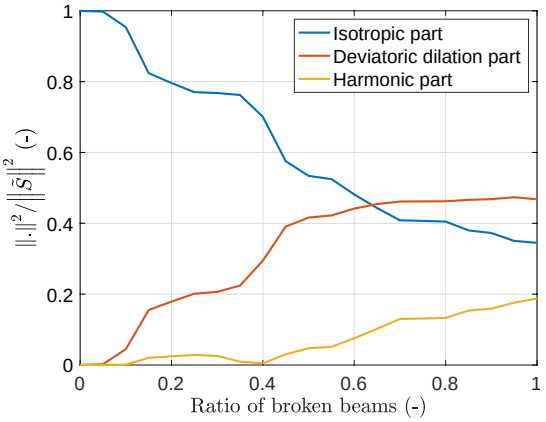

Figure 15: Simple shear loading: Evolution of the relative parts of the effective compliance tensor with the ratio of broken beams.

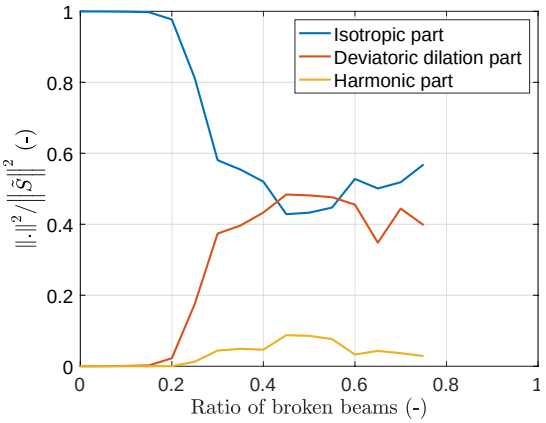

Figure 16: Willam loading: Evolution of the relative parts of the effective compliance tensor with the ratio of broken beams.

iii) After a certain level, the beams failure will be related to the direction of loading and the microcracks begin to orient themselves while remaining diffuse. The loss of isotropy implies that the $\mathbf{d}'$-related part becomes non-zero. On the other hand, the harmonic part remains null. This is a case of crack-induced orthotropy.

iv) Eventually, the cracks will start to interact or coalesce and the harmonic part becomes non-zero. So we deviate from the framework of Kachanov's theory. Depending on the symmetry class of the harmonic tensor, it can be induced orthotropy or no-symmetry induced anisotropy.

Those stages can be observed on the computed cracking patterns of figures 17 to 21.

We note that the results are very dependent on the loading studied. However, we can draw a general conclusion from the curves presented above: the effective compliance tensor is close to remain orthotropic even at very high levels of cracking. Indeed, the harmonic part of the effective compliance tensor remains negligible in most loading cases. This last observation is consistent with Kachanov dilute (non interacting) micro-cracking theory, for which the harmonic part of the compliance tensor remains zero for any network of diffuse and open micro-cracks. Furthermore, it is most often satisfied here even in cases of localizing and interacting cracks.

When this harmonic part is not negligible, as in the cases of compression (see figure 13) or shear (see figure 15), the effective compliance tensor does not necessarily becomes anisotropic without symmetry. Indeed, as it is observed in figure 11, $\tilde{\mathbf{S}}$ remains close to belong to the orthotropic symmetry class ($\Delta < 15\%$), and this up to quite high values of damage.

7. Extraction of damage tensors

A natural definition of the damage variable from the effective elasticity tensor leads to a fourth-order tensor (Chaboche, 1979; Leckie and Onat, 1980). However, the use of a symmetric second-order tensor is common due to the simplicity of its interpretation (Cordebois and Sidoroff, 1982; Murakami, 1988).

The definition of a second-order damage variable is justified here since we have checked that the elasticity tensors, and thus the fourth-order damage tensors, remain close to the orthotropic symmetric class – the symmetry class of a generic second-order tensor– even at high levels of damage. Nonetheless, the definition of such a damage variable is not straightforward. After choosing between a definition based on the compliance tensor or the stiffness tensor, one must select the degradations rendered by this damage variable, which can be related either to the bulk modulus, to the shear modulus or possibly to a combination of both.

To validate the definition of a symmetric second-order tensor as damage variable, it must be checked that it is

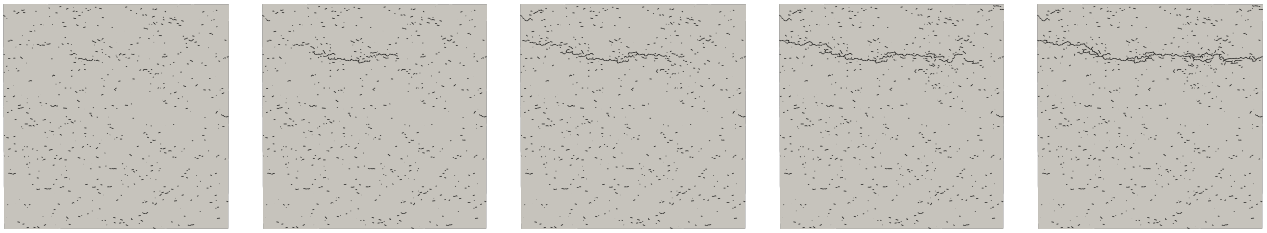

(a) 60 % (b) 70 % (c) 80 % (d) 90 % (e) 100 %

Figure 17: Tensile loading: evolution of the crack pattern with the ratio of broken beams.

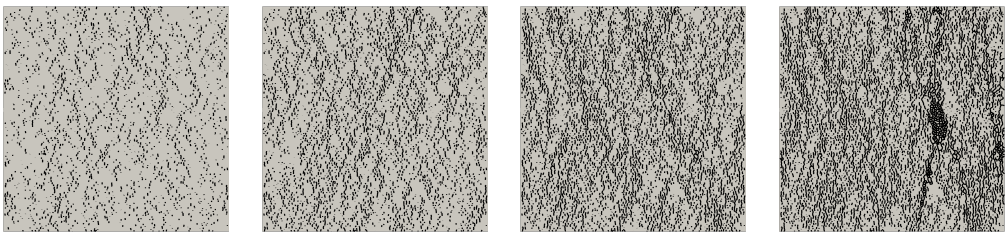

(a) 20 % (b) 40 % (c) 60 % (d) 80 %

Figure 18: Compressive loading: evolution of the crack pattern with the ratio of broken beams.

(a) 45 % (b) 55 % (c) 65 % (d) 75 % (e) 85 %

Figure 19: Bi-Tensile loading: evolution of the crack pattern with the ratio of broken beams.

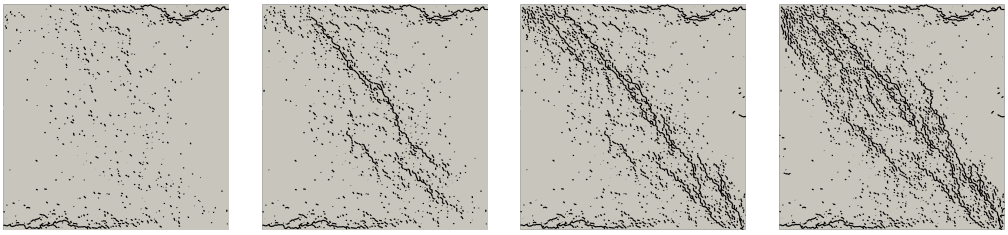

(a) 20 % (b) 40 % (c) 60 % (d) 80 %

Figure 20: Simple shear loading: evolution of the crack pattern with the ratio of broken beams.

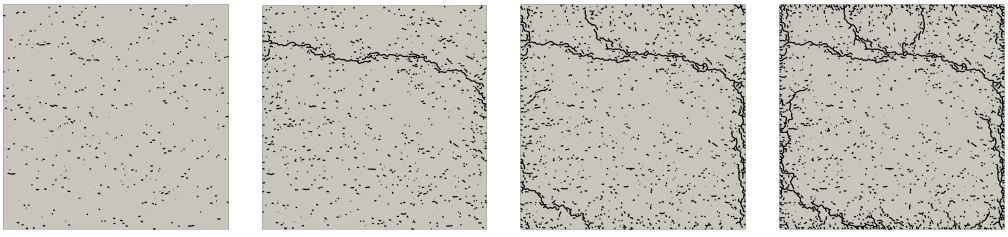

(a) 10 % (b) 30 % (c) 50 % (d) 70 %

Figure 21: Willam loading: evolution of the crack pattern with the ratio of broken beams.

positive definite, that its eigenvalue are bounded by one and that its time derivative is positive definite, the later property being related to the second principle of thermodynamics (Desmorat, 2006). One should note that those properties are verified by the fourth-order tensor per definition. This is on the other hand the modelling choices that will ensure, or not, those properties for the second-order tensor.

7.1. From compliance tensor

Following M. Kachanov, a natural definition for an anisotropic damage variable is related to the compliance tensor. More precisely, we propose here to define it from the difference between the invert of the effective bulk modulus, very sensitivitive to damage, and the invert of the initial bulk modulus,

$$\frac{1}{\tilde{\kappa}} - \frac{1}{\kappa} = \mathrm{tr}\,\mathbf{d}(\tilde{\mathbf{S}} - \mathbf{S}) = \mathrm{tr}\,\mathrm{tr}_{12}\left(\tilde{\mathbf{S}} - \mathbf{S}\right).$$

We first define a dimensionless symmetric second-order tensor,

$$\boldsymbol{\Omega} := \kappa\left(\mathbf{d}(\tilde{\mathbf{S}}) - \mathbf{d}(\mathbf{S})\right) = \kappa\,\mathrm{tr}_{12}\left(\tilde{\mathbf{S}} - \mathbf{S}\right),$$

whose trace is $\kappa/\tilde{\kappa} - 1 \geq 0$, and of eigenvalues expected to be positive but unbounded ($0 \leq \Omega_i < \infty$). A dimensionless symmetric second-order damage variable is obtained as

$$\widehat{\mathbf{D}} := \boldsymbol{\Omega}\,(\mathbf{1} + \boldsymbol{\Omega})^{-1} = (\mathbf{1} + \boldsymbol{\Omega})^{-1}\,\boldsymbol{\Omega}.$$

One should note that the eigenvalues of $\widehat{\mathbf{D}}$ remain positive and bounded by 1 provided those of $\boldsymbol{\Omega}$ are positive.

The figures 22 to 26 show the evolutions of the components of the damage tensor $\widehat{\mathbf{D}}$ with the ratio of broken beams for the studied loadings. One can see that the values of the components of $\widehat{\mathbf{D}}$ are not bounded by 0 and 1. In view of the values obtained, this is in a non surprising manner also the case for the eigenvalues. Therefore, this definition based solely on the invert of the initial bulk modulus is is not compatible with a thermodynamics framework. Indeed, it does not ensure the positivity of $\boldsymbol{\Omega}$. The most problematic cases are the compressive loading (Fig. 23) and the simple shear loading (Fig. 25), for which the evolution of the shear modulus might certainly not be easily linked to the evolution of the bulk modulus. A solution would be to introduce this shear modulus in the definition of the damage variable itself. However, this solution would be difficult to implement because one would need to introduce some parameters to combine both the bulk modulus part and the shear modulus part, parameters that will have to be identified later.

7.2. From stiffness tensor

A second – alternative and, one will see, preferred – anisotropic damage variable can be defined as related to

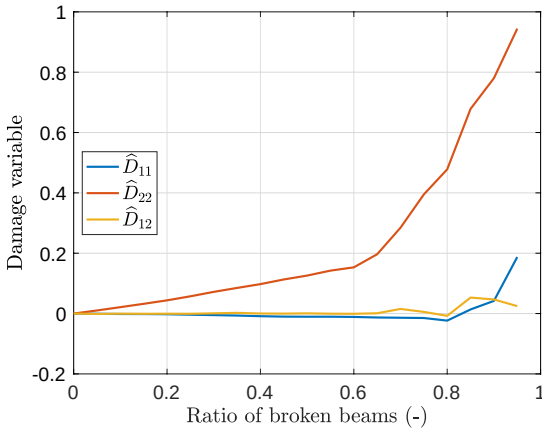

Figure 22: Tensile loading: Evolution of the components of the damage tensor $\widehat{\mathbf{D}}$ with the ratio of broken beams.

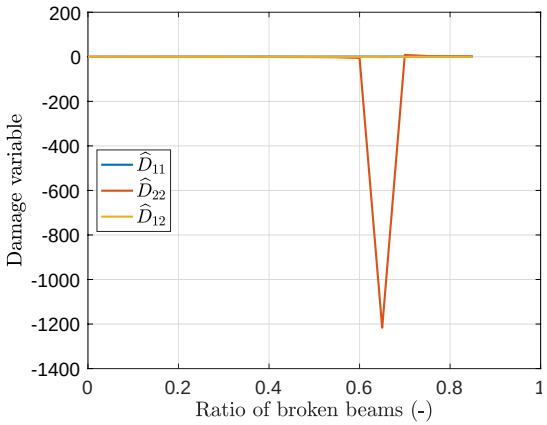

Figure 23: Compressive loading: Evolution of the components of the damage tensor $\widehat{\mathbf{D}}$ with the ratio of broken beams.

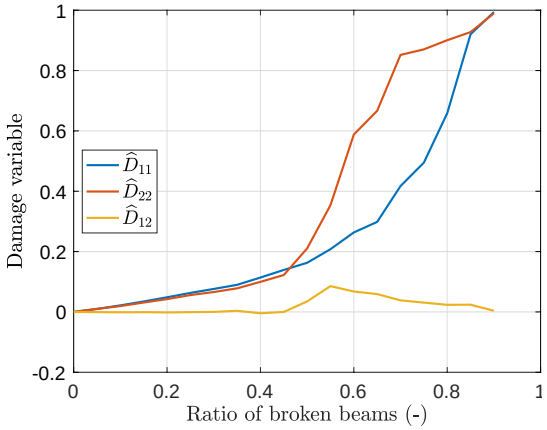

Figure 24: Bi-Tensile loading: Evolution of the components of the damage tensor $\widehat{\mathbf{D}}$ with the ratio of broken beams.

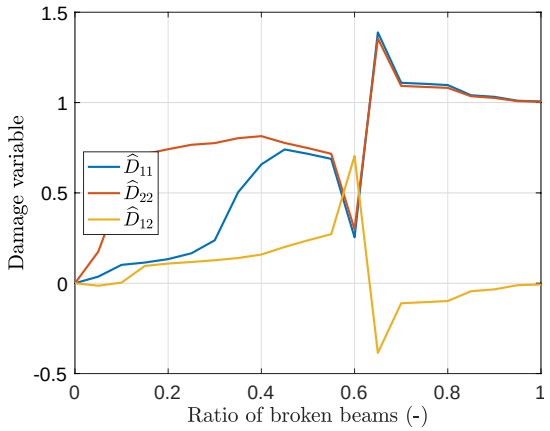

Figure 25: Simple shear loading: Evolution of the components of the damage tensor $\widehat{\mathbf{D}}$ with the ratio of broken beams.

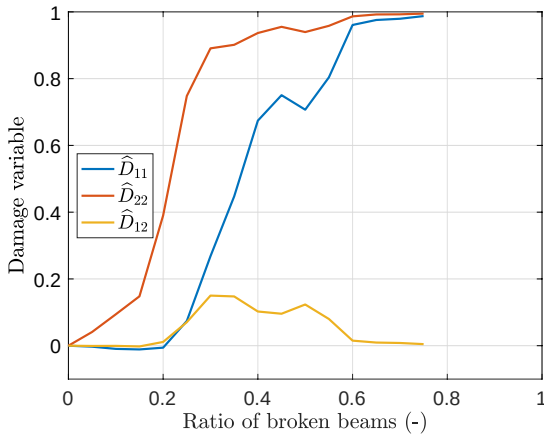

Figure 26: Willam loading: Evolution of the components of the damage tensor $\widehat{\mathbf{D}}$ with the ratio of broken beams.

the effective bulk modulus instead of its inverse, more precisely as related to the difference

$$\kappa - \tilde{\kappa} = \frac{1}{4}\,\mathrm{tr}\,\mathbf{d}(\mathbf{C} - \tilde{\mathbf{C}}) = \frac{1}{4}\,\mathrm{tr}\,\mathrm{tr}_{12}\left(\mathbf{C} - \tilde{\mathbf{C}}\right)$$

We propose to define the damage variable as the dimensionless symmetric second order tensor:

$$\begin{aligned}\mathbf{D} &:= \mathbf{d}(\mathbf{C})^{-1}\left(\mathbf{d}(\mathbf{C}) - \mathbf{d}(\tilde{\mathbf{C}})\right)\\ &= \left(\mathbf{d}(\mathbf{C}) - \mathbf{d}(\tilde{\mathbf{C}})\right)\mathbf{d}(\mathbf{C})^{-1}\end{aligned}$$

as $\mathbf{d}(\mathbf{C}) = \mathrm{tr}_{12}\,\mathbf{C} = 2\kappa\,\mathbf{1}$ is spherical due to initial isotropy, so that the previous commutativity property holds, with

$$\mathbf{D} = \frac{1}{2\kappa}\left(\mathbf{d}(\mathbf{C}) - \mathbf{d}(\tilde{\mathbf{C}})\right) = \frac{1}{2\kappa}\,\mathrm{tr}_{12}\left(\mathbf{C} - \tilde{\mathbf{C}}\right) \qquad (7.1)$$

One must check that the damage tensor $\mathbf{D}$ thus defined has positive eigenvalues bounded by 1 ($0 \leq D_i \leq 1$). The figures 27 to 31 show the evolutions of the components of the damage tensor $\mathbf{D}$ with the ratio of broken beams for the studied loadings.

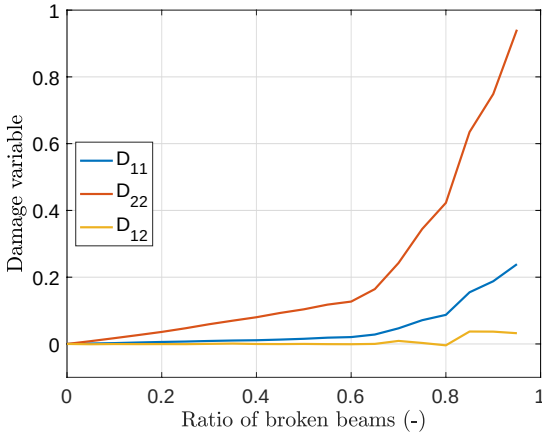

Figure 27: Tensile loading: Evolution of the components of the damage tensor $\mathbf{D}$ with the ratio of broken beams.

We can observe that, this time, the components of the second-order tensorial damage variable remain postive and bounded by 1. In most cases, a maximum damage close to 1 is reached on at least one of the tensor components before the end of the loading. This may explain why it is no longer possible to extract the effective elasticity tensors even though the ratio of broken beams has not yet reached 1.

In pure proportional loading we expect a strict increase in the components of the tensor damage variable. This is not always the case. Indeed, in the case of bi-tension (Fig. 29) and simple shear (Fig. 30), the slight decreases of the shear component D_{12} is mainly related to local non proportionality (and rotation of the principal axes of tensor $\mathbf{D}$). The drop is clear in the Willam loading case (see figure 31). However, the damage eigenvalues D_1, D_2 of $\mathbf{D}$ always increase for this loading as illustrated in figure 32.

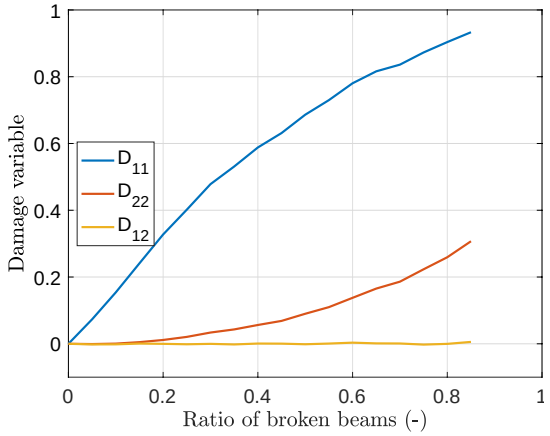

Figure 28: Compressive loading: Evolution of the components of the damage tensor $\mathbf{D}$ with the ratio of broken beams.

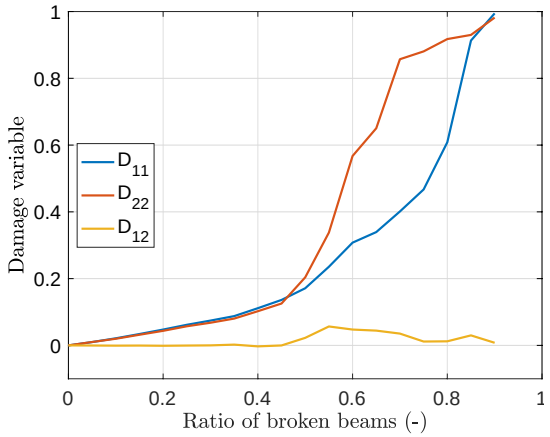

Figure 29: Bi-Tensile loading: Evolution of the components of the damage tensor $\mathbf{D}$ with the ratio of broken beams.

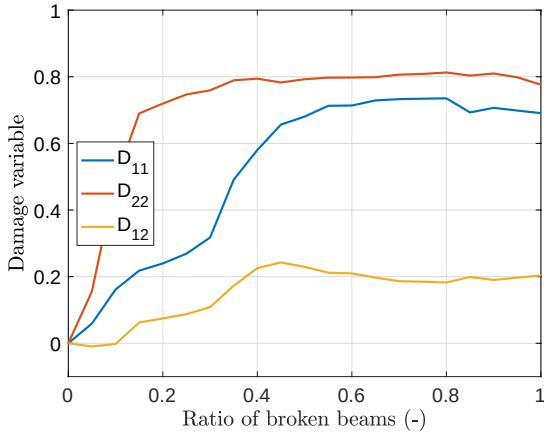

Figure 30: Simple shear loading: Evolution of the components of the damage tensor $\mathbf{D}$ with the ratio of broken beams.

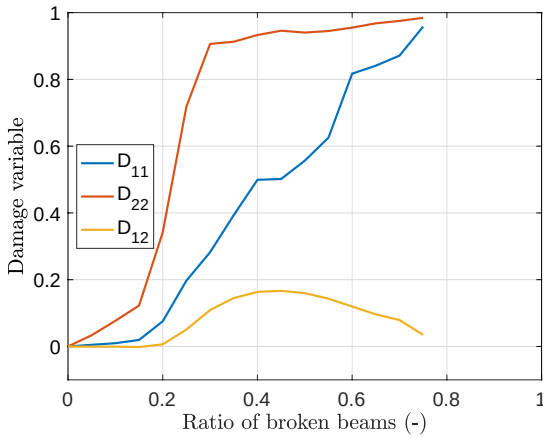

Figure 31: Willam loading: Evolution of the components of the damage tensor $\mathbf{D}$ with the ratio of broken beams.

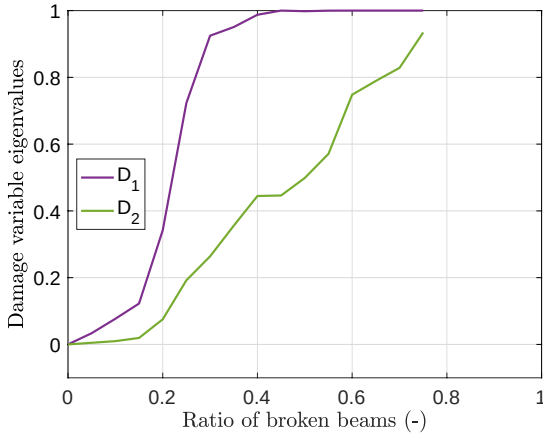

Figure 32: Willam loading: Evolution of the eigenvalues of the damage tensor $\mathbf{D}$ with the ratio of broken beams.

8. Conclusion

An upper bound to the distance to orthotropy has been obtained for bi-dimensional elasticity tensors. It naturally introduces a second –instead of fourth– order tensor which models the medium orthotropy. This has allowed us to propose and measure second order tensorial damages variables fully representative of the effective anisotropic degradation due to complex cracking patterns. We have performed 2D discrete simulations with a beam-particle model of initially isotropic Representative Area Elements, allowing for strong interactions between cracks (up to their coalescence and complete failure). We have analyzed these simulations in a systematic manner.

The results associated with the discrete computations confirm the accuracy of the orthotropic approximation of the elasticity tensor for a 2D cracked medium, under both proportional or non-proportional loading cases. They fully justify the use of a single second order damage tensor variable, instead of a fourth order one (Chaboche, 1979; Leckie and Onat, 1980) or of two second order damage variables (Desmorat and Desmorat, 2016), even in the strong crack interaction case.

Two definitions, in stiffness and in compliance, for a symmetric second-order damage tensor have been proposed and studied in this paper. They are both based on the evolution of the bulk modulus (or of its inverse). It has been observed that the damage variable derived from the stiffness tensor has the necessary properties to be a suitable candidate for the formulation of a continuous anisotropic damage model in 2D from discrete simulations.

The methodology followed does not fix *a priori* a particular working basis, it makes accessible all the tensorial (multiaxial) components measurement of the damage variable are any time step, therefore of its evolution.

Appendix A. Harmonic square roots of bi-dimensional harmonic tensors

The goal of this appendix is to provide a simple proof of the following theorem, using results in (Desmorat et al., 2020).

Theorem Appendix A.1. *Any fourth-order harmonic bi-dimensional tensor* $\mathbf{H}$ *can be written either as an harmonic product* $\mathbf{h}*\mathbf{h}$ *(an harmonic square), or as* $-\mathbf{k}*\mathbf{k}$ *(the opposite of an harmonic square), where* $\mathbf{h}$ *and* $\mathbf{k}$ *are second-order bi-dimensional harmonic tensors.*

To prove this result, we will recall first that there is an isomorphism $\mathbf{H} \cong \mathrm{h}$ between bi-dimensional harmonic tensors $\mathbf{H}$ of order n and homogeneous harmonic polynomials h of degree n in two variables x and y. Rather than x and y, one can use the complex variables $z = x + iy$ and $\bar{z} = x - iy$. Then, any homogeneous harmonic polynomial of degree n writes as $\mathrm{h}_1 = \mathfrak{Re}(\bar{z}_1 z^n)$, where $z_1 \in \mathbb{C}$ and the harmonic product between two homogeneous harmonic polynomials h_1 and h_2, of respective degree n_1 and n_1 translates into

$$\mathrm{h}_1 * \mathrm{h}_2 = \frac{1}{2}\,\mathfrak{Re}(\overline{z_1 z_2} z^{n_1+n_2}).$$

For instance, the deviatoric second order tensors

$$\mathbf{h} = \begin{pmatrix} a_1 & b_1 \\ b_1 & -a_1 \end{pmatrix} \quad \text{and} \quad \mathbf{k} = \begin{pmatrix} a_2 & b_2 \\ b_2 & -a_2 \end{pmatrix}$$

are represented respectively by the harmonic polynomials

$$\mathrm{h}_1 = \mathfrak{Re}(\bar{z}_1 z^2), \quad \text{and} \quad \mathrm{h}_2 = \mathfrak{Re}(\bar{z}_2 z^2),$$

where $z_1 = a_1 + ib_1$ and $z_2 = a_2 + ib_2$, and an harmonic fourth order tensor $\mathbf{H}$ (represented by its Kelvin matrix (3.1)) corresponds to the homogeneous harmonic polynomial $\mathrm{h}_3 = \mathfrak{Re}(\bar{z}_3 z^4)$, where

$$z_3 = H_{1111} + iH_{1112}.$$

Thus, the harmonic square tensorial equations

$$\mathbf{H} = \mathbf{h} * \mathbf{h} = -\mathbf{k} * \mathbf{k}$$

translate, in terms of harmonic homogeneous polynomials, as

$$\mathrm{h}_3 = \mathfrak{Re}(\bar{z}_3 z^4) = \mathfrak{Re}(\bar{z}_1^2 z^4) = -\,\mathfrak{Re}(\bar{z}_2^2 z^4).$$

and the solutions are provided by roots of the algebraic equations

$$z_1^2 = -z_2^2 = z_3. \tag{A.1}$$

Remark Appendix A.2. Note that both equations $\mathbf{H} = \mathbf{h}*\mathbf{h}$ and $\mathbf{H} = -\mathbf{k}*\mathbf{k}$ have exactly two opposite solutions, when $\mathbf{H} \neq 0$.

References

André, D., Iordanoff, I., Charles, J.l., Néauport, J., 2012. Discrete element method to simulate continuous material by using the cohesive beam model. Computer methods in applied mechanics and engineering 213, 113–125.

Backus, G., 1970. A geometrical picture of anisotropic elastic tensors. Reviews of geophysics 8, 633–671.

Bagi, K., 1996. Stress and strain in granular assemblies. Mechanics of materials 22, 165–177.

Chaboche, J.L., 1979. Le concept de contrainte effective appliqué à l'élasticité et à la viscoplasticité en présence d'un endommagement anisotrope, in: Boehler, J.P. (Ed.), Colloque Int. CNRS 295, Villard de Lans, Martinus Nijhoff Publishers and Editions du CNRS, 1982. pp. 737–760.

Challamel, N., Picandet, V., Pijaudier-Cabot, G., 2015. From discrete to nonlocal continuum damage mechanics: Analysis of a lattice system in bending using a continualized approach. International Journal of Damage Mechanics 24, 983–1012.

Cordebois, J., Sidoroff, F., 1982. Endommagement anisotrope en élasticité et plasticité. J. Meca. Th. Appl., Special Volume , 45–65.

Cundall, P.A., Strack, O.D., 1979. A discrete numerical model for granular assemblies. geotechnique 29, 47–65.

D'Addetta, G.A., Kun, F., Ramm, E., 2002. On the application of a discrete model to the fracture process of cohesive granular materials. Granular Matter 4, 77–90.

Delaplace, A., 2008. Modélisation discrète appliquée au comportement des matériaux et des structures. Mémoire d'habilitation à diriger des recherches de l'Ecole Normale Supérieure de Cachan .

Delaplace, A., Desmorat, R., 2007. Discrete 3d model as complimentary numerical testing for anisotropic damage. Int J Fract 148, 115–128.

Desmorat, B., Desmorat, R., 2015. Tensorial polar decomposition of 2d fourth-order tensors. Comptes Rendus Mécanique 343, 471–475.

Desmorat, B., Desmorat, R., 2016. Second order tensorial framework for 2d medium with open and closed cracks. European Journal of Mechanics-A/Solids 58, 262–277.

Desmorat, B., Olive, M., Auffray, N., Desmorat, R., Kolev, B., 2020. Computation of minimal covariants bases for 2d coupled constitutive laws. arXiv preprint arXiv:2007.01576 .

Desmorat, R., 2006. Positivity of intrinsic dissipation of a class of nonstandard anisotropic damage models. C. R. Mecanique 334, 587–592.

Desmorat, R., 2016. Anisotropic damage modeling of concrete materials. International Journal of Damage Mechanics 25, 818–852.

Desmorat, R., Gatuingt, F., Ragueneau, F., 2007. Nonlocal anisotropic damage model and related computational aspects for quasi-brittle materials. Engineering Fracture Mechanics 74, 1539–1560.

Halm, D., Dragon, A., 1998. An anisotropic model of damage and frictional sliding for brittle materials. European Journal of Mechanics-A/Solids 17, 439–460.

Herrmann, H.J., Hansen, A., Roux, S., 1989. Fracture of disordered, elastic lattices in two dimensions. Physical Review B 39, 637.

Hrennikoff, A., 1941. Solution of problems of elasticity by the framework method. J. appl. Mech. .

Jivkov, A., 2014. Structure of micro-crack population and damage evolution in quasi-brittle media. Theoretical and Applied Fracture Mechanics 70, 1–9.

Kachanov, M., 1992. Effective elastic properties of cracked solids: critical review of some basic concepts. Appl. Mech. Rev. 45, 304–335.

Leckie, F., Onat, E., 1981. Tensorial nature of damage measuring internal variables, in: Physical non-linearities in structural analysis. Springer, pp. 140–155.

Leckie, F.A., Onat, E.T., 1980. Tensorial nature of damage measuring internal variables. J. Hult and J. Lemaitre eds, Springer Berlin. chapter Physical Non-Linearities in Structural Analysis. pp. 140–155.

Lemaitre, J., Chaboche, J.L., 1985. Mécanique des matériaux solides. Dunod, english translation 1990 'Mechanics of Solid Materials' Cambridge University Press.

Lemaitre, J., Desmorat, R., 2005. Engineering damage mechanics: ductile, creep, fatigue and brittle failures. Springer Science & Business Media.

Mazars, J., 1984. Application de la mécanique de l'endommagement au comportement non linéaire et à la rupture du béton de structure. Ph.D. thesis. Université Pierre et Marie Curie - Paris 6.

Mazars, J., Berthaud, Y., Ramtani, S., 1990. The unilateral behaviour of damaged concrete. Engineering Fracture Mechanics 35, 629–635.

Meguro, K., Hakuno, M., 1989. Fracture analyses of concrete structures by the modified distinct element method. Doboku Gakkai Ronbunshu 1989, 113–124.

Murakami, S., 1988. Mechanical modeling of material damage. ASME J. Appl. Mech. 55, 280–286. doi:10.1115/1.3173673.

Olive, M., Kolev, B., Desmorat, B., Desmorat, R., 2018a. Harmonic factorization and reconstruction of the elasticity tensor. Journal of Elasticity 132, 67–101.

Olive, M., Kolev, B., Desmorat, R., Desmorat, B., 2018b. Characterization of the symmetry class of an elasticity tensor using polynomial covariants. arXiv:1807.08996 [math.RT] .

Oliver-Leblond, C., 2019. Discontinuous crack growth and toughening mechanisms in concrete: A numerical study based on the beam-particle approach. Engineering Fracture Mechanics 207, 1–22.

Poisson, S.D., 1828. Mémoire sur l'équilibre et le mouvement des corps élastiques. F. Didot.

Ramtani, S., Berthaud, Y., Mazars, J., 1992. Orthotropic behavior of concrete with directional aspects: modelling and experiments. Nuclear Engineering and design 133, 97–111.

Rinaldi, A., 2013. Bottom-up modeling of damage in heterogeneous quasi-brittle solids. Continuum Mechanics and Thermodynamics 25, 359–373.

Rinaldi, A., Lai, Y.C., 2007. Statistical damage theory of 2d lattices: Energetics and physical foundations of damage parameter. International Journal of Plasticity 23, 1796–1825.

Schlangen, E., Van Mier, J.G.M., 1992. Simple lattice model for numerical simulation of fracture of concrete materials and structures. Materials and Structures 25, 534–542.

Schouten, J.A., 1989. Tensor analysis for physicists. Courier Corporation.

Spencer, A., 1970. A note on the decomposition of tensors into traceless symmetric tensors. International Journal of Engineering Science 8, 475–481.

Tillemans, H.J., Herrmann, H.J., 1995. Simulating deformations of granular solids under shear. Physica A: Statistical Mechanics and its Applications 217, 261–288.

Vannucci, P., 2005. Plane anisotropy by the polar method. Meccanica 40, 437–454.

Vannucci, P., Verchery, G., 2001. Stiffness design of laminates using the polar method. International Journal of Solids and Structures 38, 9281–9894. doi:10.1016/S0020-7683(01)00177-9.

Vassaux, M., Oliver-Leblond, C., Richard, B., Ragueneau, F., 2016. Beam-particle approach to model cracking and energy dissipation in concrete: Identification strategy and validation. ICement and Concrete Composites 70, 1–14.

Vassaux, M., Richard, B., Ragueneau, F., Millard, A., 2015a. Regularised crack behaviour effects on continuum modelling of quasi-brittle materials under cyclic loading. Engineering Fracture Mechanics 149, 18–36.

Vassaux, M., Richard, B., Ragueneau, F., Millard, A., Delaplace, A., 2015b. Lattice models applied to cyclic behavior description of quasi-brittle materials: advantages of implicit integration. International Journal for Numerical and Analytical Methods in Geomechanics 39, 775–798.

Verchery, G., 1982. Les invariants des tenseurs d'ordre 4 du type de l'élasticité, in: Mechanical behavior of anisotropic solids/comportment Méchanique des Solides Anisotropes. Springer, pp. 93–104.

Vianello, M., 1997. An integrity basis for plane elasticity tensors. Archives of Mechanics 49, 197–208.

Willam, K., Pramono, E., Sture, S., 1989. Fundamental issues of smeared crack models, in: Fracture of concrete and rock. Springer, pp. 142–157.